

RECEIVED: May 29, 2014

REVISED: July 30, 2014

ACCEPTED: July 31, 2014

PUBLISHED: August 21, 2014

Understanding the correlation between $(g - 2)_\mu$ and $\mu \rightarrow e\gamma$ in the MSSM

Jörn Kersten,^{a,b} Jae-hyeon Park,^c Dominik Stöckinger^d and Liliana Velasco-Sevilla^a

^aUniversity of Hamburg, II. Institute for Theoretical Physics,
Luruper Chaussee 149, 22761 Hamburg, Germany

^bUniversity of Bergen, Department of Physics and Technology,
PO Box 7803, 5020 Bergen, Norway

^cDepartament de Física Teòrica and IFIC, Universitat de València-CSIC,
46100, Burjassot, Spain

^dInstitut für Kern- und Teilchenphysik, TU Dresden, 01069 Dresden, Germany

E-mail: joern.kersten@desy.de, jae.park@uv.es,

Dominik.Stoekinger@tu-dresden.de, liliana.velascosevilla@gmail.com

ABSTRACT: The supersymmetric contributions to the muon anomalous magnetic moment a_μ and to the decay $\mu \rightarrow e\gamma$ are given by very similar Feynman diagrams. Previous works reported correlations in specific scenarios, in particular if a_μ is dominated by a single diagram. In this work we give an extensive survey of the possible correlations. We discuss examples of single-diagram domination with particularly strong correlations, and provide corresponding benchmark parameter points. We show how the correlations are weakened by significant cancellations between diagrams in large parts of the MSSM parameter space. Nevertheless, the order of magnitude of $\text{BR}(\mu \rightarrow e\gamma)$ for a fixed flavor-violating parameter can often be predicted. We summarize the behavior by plotting the correlations as well as resulting bounds on the flavor-violating parameters under various assumptions on the MSSM spectrum.

KEYWORDS: Supersymmetry Phenomenology

ARXIV EPRINT: [1405.2972](https://arxiv.org/abs/1405.2972)

Contents

1	Introduction	1
2	Status of relevant observables	2
2.1	$(g - 2)_\mu$ and $\text{BR}(\mu \rightarrow e\gamma)$	2
2.2	Superparticle masses	3
3	Contributions to a_μ and $a_{\mu e\gamma}$	4
3.1	Chargino-sneutrino contributions	4
3.2	Neutralino-charged slepton contributions	5
4	Correlations in different parameter space regions	7
4.1	Similar SUSY masses	7
4.2	Chargino dominance	8
4.3	Large μ limit	16
4.4	Neutralino- $\tilde{\mu}_R$ dominance	20
5	Discussion and main results	22
5.1	Correlation between a_μ and $\text{BR}(\mu \rightarrow e\gamma)$ for similar supersymmetric masses	22
5.2	Specific results for the case of chargino dominance	24
5.3	Specific results for cases with neutralino dominance	26
5.4	Comparison of different scenarios	26

1 Introduction

As is well established, the Minimal Supersymmetric Standard Model (MSSM) with fully general soft supersymmetry (SUSY) breaking parameters is strongly constrained by flavor-violating observables. Particularly in the charged lepton sector no sign of flavor violation has been observed yet. In contrast, the muon anomalous magnetic moment $a_\mu = (g_\mu - 2)/2$ is a flavor-conserving leptonic observable with a tantalizing deviation Δa_μ between experiment and Standard Model (SM) prediction by more than 3σ , which could be explained beautifully by the contributions from light sleptons, charginos, or neutralinos. On the other hand, the Feynman diagrams for SUSY contributions to a_μ and to the branching ratio of the flavor-violating decay $\mu \rightarrow e\gamma$, $\text{BR}(\mu \rightarrow e\gamma)$, are essentially identical, except for the flavor transition appearing only in the latter case. For this reason it was put forward to study correlations between the two observables in the MSSM [1–3].

Such correlations could prove useful, for example, in constraining scenarios which are in agreement with a_μ . Once the SUSY contribution to a_μ is fixed, the mass scale of the relevant superparticles is fixed as well. One could then predict the value of $\text{BR}(\mu \rightarrow e\gamma)$ as a function

of only the flavor-violating SUSY breaking parameters and thus derive stringent bounds on these parameters, which cannot be evaded by simply raising the overall SUSY mass scale. It has already been noted in [2] that a strong correlation could emerge if the contribution to a_μ comes mainly from a single diagram; a strong correlation was also observed in [3] in a parameter scan. The interest of the present work is to identify the parameter space where this happens. In fact, cases with a strong correlation often correspond to certain mass hierarchies among the particles involved. Hence we characterize such hierarchies and establish the corresponding bounds.

On the other hand, in large parts of the MSSM parameter space the SUSY contribution to a_μ is large but no single contribution to a_μ dominates. It is then also of interest to study to what extent the two observables are correlated and whether we can derive bounds on the flavor-violating parameters even in such cases.

Motivated by the stringent LHC mass limits on colored SUSY particles, which in constrained scenarios imply stringent limits also on uncolored superparticles, we consider the MSSM without assumptions on GUT-scale or SUSY breaking physics. For our study, only electroweak parameters are relevant: the higgsino and gaugino mass parameters μ , M_1 , M_2 , the ratio of the Higgs vacuum expectation values $\tan\beta$, and the slepton mass and mixing parameters, to be described below.

The work is organized as follows. In section 2 we present the status of the relevant observables. In section 3 we discuss the SUSY contributions to a_μ and $\text{BR}(\mu \rightarrow e\gamma)$. In section 4.1, we survey their correlation in the general case where all supersymmetric particles involved in a_μ and $\mu \rightarrow e\gamma$ have no particular hierarchy. For this case the charginos tend to dominate, so in section 4.2 we study the conditions under which correlations between a_μ and $\text{BR}(\mu \rightarrow e\gamma)$ could be established for chargino domination. In section 4.3 we study a scenario where the μ parameter is very large and the lightest neutralino is essentially a bino, so the main contribution to a_μ is given by diagrams involving binos, $\tilde{\mu}_L$, and $\tilde{\mu}_R$. Finally, in section 4.4 we consider the case where all left-handed sleptons are very heavy, so that the chargino and most neutralino contributions are suppressed, except for the neutralino contribution with $\tilde{\mu}_R$ exchange.

Section 5 can be read independently. It provides an extended discussion of the results, and it summarizes the behavior with plots of the correlations and bounds on flavor-violating parameters under various assumptions on the SUSY spectrum.

2 Status of relevant observables

2.1 $(g - 2)_\mu$ and $\text{BR}(\mu \rightarrow e\gamma)$

The difference between the experimental determination [4] and the SM prediction for the anomalous magnetic moment of the muon is larger than 3σ . Taking the evaluation of hadronic contributions of ref. [5], including recent updates of the QED [6] and electroweak [7] contributions, and adding theoretical and experimental uncertainties in quadrature, the difference is

$$\Delta a_\mu = a_\mu^{\text{exp}} - a_\mu^{\text{SM}} = (287 \pm 80) \times 10^{-11}. \quad (2.1)$$

Alternative theory evaluations [8, 9] obtain similar or even larger differences. Further progress can be expected not only from improvements on the theory side, but in particular from Fermilab P989 [10, 11] and the new J-PARC approach to the $g - 2$ /EDM measurements [12]. Both aim to improve the experimental uncertainty of a_μ by at least a factor of 4.

In quantum field theory, a_μ can be obtained from the covariant decomposition of the muon-photon three-point function. Written similarly to [2], the relevant term is

$$\mathcal{M}_\mu = \frac{e}{2m_\mu} \epsilon^\alpha \bar{u}_\mu(k+q) [iq^\beta \sigma_{\beta\alpha} a_\mu] u_\mu(k), \quad (2.2)$$

in the limit $q \rightarrow 0$. Here $\sigma_{\alpha\beta} = i/2 [\gamma_\alpha, \gamma_\beta]$, ϵ^α is the photon polarization vector, k and $k+q$ are on-shell momenta, and finally u_μ , \bar{u}_μ are spinors that satisfy the Dirac equation.

The current 90% C.L. upper limit on the branching ratio $\text{BR}(\mu \rightarrow e\gamma)$, set by the MEG experiment [13], is

$$\text{BR}(\mu \rightarrow e\gamma) < 5.7 \times 10^{-13} \equiv \text{BR}_{\text{EXP}}(\mu \rightarrow e\gamma), \quad (2.3)$$

and future upgrades will attempt to explore regions of $O(10^{-14})$ [14]. We write the amplitude for $\mu \rightarrow e\gamma$ as

$$\mathcal{M}_{\mu e\gamma} = \frac{e}{2m_\mu} \epsilon^{*\alpha} \bar{u}_e(k+q) [i\sigma_{\beta\alpha} q^\beta (a_{\mu e\gamma R} P_L + a_{\mu e\gamma L} P_R)] u_\mu(k), \quad (2.4)$$

where $P_{R,L} = (1 \pm \gamma_5)/2$. The L/R index in $a_{\mu e\gamma L/R}$ refers to the electron chirality. Thus, L and R are interchanged with respect to the notation in [2, 15]. By convention, the photon momentum q is oriented towards the vertex in both eq. (2.2) and eq. (2.4). The resulting branching ratio is

$$\text{BR}(\mu \rightarrow e\gamma) = \frac{3\pi^2 e^2}{G_F^2 m_\mu^4} (|a_{\mu e\gamma L}|^2 + |a_{\mu e\gamma R}|^2). \quad (2.5)$$

2.2 Superparticle masses

While the negative results from LHC SUSY searches place stringent lower limits on the masses of the colored superparticles, the electroweakly interacting charginos, neutralinos and sleptons are still allowed to be quite light [16–20]. This is very enthralling because a sizable supersymmetric contribution to the muon $g - 2$ requires masses of $\mathcal{O}(100)$ GeV precisely for sleptons and charginos or neutralinos. Consequently, within the general MSSM an appealing possibility is to consider scenarios with the hierarchy

$$m_{\tilde{q}}, m_{\tilde{g}} \gg m_{\tilde{l}}, m_{\tilde{\chi}^\pm}, m_{\tilde{\chi}^0}. \quad (2.6)$$

Collider constraints on the masses relevant for a_μ and $\mu \rightarrow e\gamma$ for certain specific scenarios of this kind were derived in [16, 21]. In particular in [21] the recent results on the searches for the non-colored supersymmetric particles were investigated in the parameter region where the muon $g - 2$ is explained. Under the assumption of the GUT relation $M_1 \approx M_2/2$, lower bounds of around 150–200 GeV were obtained for the wino mass. Further, refs. [22, 23] revealed logarithmically enhanced two-loop corrections from mass hierarchies

such as those in eq. (2.6). Since we will focus on the parametric dependence of a_μ , $\text{BR}(\mu \rightarrow e\gamma)$ and their correlation on the SUSY spectrum, we will choose parameters satisfying eq. (2.6) but we will not use more detailed LHC mass limits and restrict ourselves to one-loop accuracy.

3 Contributions to a_μ and $a_{\mu e\gamma}$

3.1 Chargino-sneutrino contributions

The one-loop contributions to $g - 2$ in the MSSM have been evaluated in full generality in [24]. If the mixing of sneutrinos of the first two generations can be decoupled from the mixing of the third generation, the contributions to $g - 2$ from a chargino $\tilde{\chi}_k^\pm$ can be nicely decomposed into two terms

$$a_\mu^{\tilde{\chi}_k^\pm} = a_\mu^{\tilde{\chi}_k^\pm}{}_1 + a_\mu^{\tilde{\chi}_k^\pm}{}_2 \tag{3.1}$$

with

$$\begin{aligned} \frac{16\pi^2}{m_\mu} a_\mu^{\tilde{\chi}_k^\pm}{}_1 &= \frac{m_\mu}{12m_{\tilde{\chi}_k^\pm}^2} (g_2^2 |V_{k1}|^2 + Y_\mu^2 |U_{k2}|^2) [\sin^2 \theta_{\tilde{\nu}} x_{k1} F_1^C(x_{k1}) + \cos^2 \theta_{\tilde{\nu}} x_{k2} F_1^C(x_{k2})], \\ \frac{16\pi^2}{m_\mu} a_\mu^{\tilde{\chi}_k^\pm}{}_2 &= -\frac{2}{3m_{\tilde{\chi}_k^\pm}} g_2 Y_\mu \text{Re}[V_{k1} U_{k2}] [\sin^2 \theta_{\tilde{\nu}} x_{k1} F_2^C(x_{k1}) + \cos^2 \theta_{\tilde{\nu}} x_{k2} F_2^C(x_{k2})], \end{aligned} \tag{3.2}$$

which correspond to the diagrams mediated by winos or higgsinos, and a combination of higgsino and wino, respectively, and which involve corresponding powers of the gauge and muon Yukawa couplings g_2 and Y_μ . Throughout this work we use the conventions of [25] unless specified otherwise. For completeness, the well-known functions F_1^C and F_2^C are defined as

$$\begin{aligned} F_1^C(x) &= \frac{2}{(1-x)^4} [2 + 3x - 6x^2 + x^3 + 6x \ln x], \\ F_2^C(x) &= -\frac{3}{2(1-x)^3} [3 - 4x + x^2 + 2 \ln x]; \end{aligned} \tag{3.3}$$

the arguments x_{ki} are defined as the mass ratios

$$x_{ki} \equiv \frac{m_{\tilde{\chi}_k^\pm}^2}{m_{\tilde{\nu}_i}^2}. \tag{3.4}$$

The sneutrino mass eigenvalues $m_{\tilde{\nu}_i}$ and the mixing angle between the first two generations, $\theta_{\tilde{\nu}}$, are defined via diagonalization of the sneutrino mass matrix,

$$\begin{aligned} \begin{pmatrix} \cos \theta_{\tilde{\nu}} & \sin \theta_{\tilde{\nu}} \\ -\sin \theta_{\tilde{\nu}} & \cos \theta_{\tilde{\nu}} \end{pmatrix} \begin{pmatrix} m_{\tilde{L}_{11}}^2 + \mathcal{D}_L^\nu & m_{\tilde{L}_{12}}^2 \\ m_{\tilde{L}_{12}}^2 & m_{\tilde{L}_{22}}^2 + \mathcal{D}_L^\nu \end{pmatrix} \begin{pmatrix} \cos \theta_{\tilde{\nu}} & -\sin \theta_{\tilde{\nu}} \\ \sin \theta_{\tilde{\nu}} & \cos \theta_{\tilde{\nu}} \end{pmatrix} &= \text{diag}(m_{\tilde{\nu}_1}^2, m_{\tilde{\nu}_2}^2) \\ \Rightarrow \tan 2\theta_{\tilde{\nu}} &= \frac{2m_{\tilde{L}_{12}}^2}{m_{\tilde{L}_{11}}^2 - m_{\tilde{L}_{22}}^2}, \end{aligned} \tag{3.5}$$

and the requirement that $\tilde{\nu}_1$ be the mass eigenstate composed primarily of $\tilde{\nu}_e$, which implies that $m_{\tilde{\nu}_1}$ is not necessarily smaller than $m_{\tilde{\nu}_2}$. Here m_{L11}^2 , m_{L22}^2 , m_{L12}^2 are the flavor-diagonal and off-diagonal soft mass parameters, and \mathcal{D}'_L are the D -term contributions to the masses. For the chargino mass matrix $M_{\tilde{\chi}^\pm}$ we use the diagonalization

$$U^* M_{\tilde{\chi}^\pm} V^\dagger = \text{diag}(m_{\tilde{\chi}_1^\pm}, m_{\tilde{\chi}_2^\pm}). \quad (3.6)$$

In the following we will neglect terms suppressed by two powers of the muon Yukawa coupling or by the electron Yukawa coupling. Then, as pointed out in [2], the right-handed part of the $\mu \rightarrow e\gamma$ amplitude vanishes,

$$a_{\mu e\gamma R}^{\tilde{\chi}_k^\pm} = 0. \quad (3.7)$$

And for the left-handed part we can write

$$a_{\mu e\gamma L}^{\tilde{\chi}_k^\pm} = a_{\mu e\gamma 1}^{\tilde{\chi}_k^\pm} + a_{\mu e\gamma 2}^{\tilde{\chi}_k^\pm}, \quad (3.8)$$

where for each chargino and for each of the two contributions in eqs. (3.1) and (3.8), the ratio of the left-handed $\mu \rightarrow e\gamma$ amplitude and a_μ takes the compact form

$$\frac{a_{\mu e\gamma I}^{\tilde{\chi}_k^\pm}}{a_{\mu I}^{\tilde{\chi}_k^\pm}} = \frac{\sin 2\theta_{\tilde{\nu}}}{2} \frac{x_{k1} F_I^C(x_{k1}) - x_{k2} F_I^C(x_{k2})}{\sin^2 \theta_{\tilde{\nu}} x_{k1} F_I^C(x_{k1}) + \cos^2 \theta_{\tilde{\nu}} x_{k2} F_I^C(x_{k2})}, \quad I = 1, 2. \quad (3.9)$$

We can rewrite this ratio as

$$\frac{a_{\mu e\gamma I}^{\tilde{\chi}_k^\pm}}{a_{\mu I}^{\tilde{\chi}_k^\pm}} = \frac{m_{L12}^2}{m_{\tilde{\nu}_1}^2 - m_{\tilde{\nu}_2}^2} \frac{\Delta_I}{x_{k2} F_I^C(x_{k2}) + \sin^2 \theta_{\tilde{\nu}} \Delta_I}, \quad (3.10)$$

where $\Delta_I \equiv x_{k1} F_I^C(x_{k1}) - x_{k2} F_I^C(x_{k2})$. We will use this result to derive analytical approximations later on.

3.2 Neutralino-charged slepton contributions

The contributions from the neutralinos and charged sleptons can be decomposed similarly to the chargino-sneutrino contributions, but the mixing structure is more complicated. Even if only the first two generations are allowed to mix, the relevant mixing of the left- and right-handed charged sleptons is described by a 4×4 matrix. In [2], this matrix was diagonalized approximately. In the following analysis, we consider the full mixing structure. Then, the neutralino contributions to a_μ can be written as (compare ref. [25] for the flavor-diagonal result)

$$\begin{aligned} \frac{16\pi^2}{m_\mu} a_\mu^{\tilde{\chi}_i^0} = & \sum_m \left[-\frac{m_\mu}{12m_{\tilde{\chi}_i^0}^2} [n_{\mu im}^{L*} n_{\mu im}^L + n_{\mu im}^R n_{\mu im}^{R*}] x_{im} F_1^N(x_{im}) \right. \\ & \left. + \frac{1}{3m_{\tilde{\chi}_i^0}} \text{Re}[n_{\mu im}^L n_{\mu im}^R] x_{im} F_2^N(x_{im}) \right]. \end{aligned} \quad (3.11)$$

Neglecting Yukawa-suppressed terms like in the chargino case, the $\mu \rightarrow e\gamma$ amplitudes can be written as

$$\begin{aligned} \frac{16\pi^2}{m_\mu} a_{\mu e\gamma R}^{\tilde{\chi}_i^0} &= \sum_m \left[-\frac{m_\mu}{12m_{\tilde{\chi}_i^0}^2} n_{\mu im}^R n_{eim}^{R*} x_{im} F_1^N(x_{im}) + \frac{1}{3m_{\tilde{\chi}_i^0}} n_{\mu im}^{L*} n_{eim}^{R*} x_{im} F_2^N(x_{im}) \right], \\ \frac{16\pi^2}{m_\mu} a_{\mu e\gamma L}^{\tilde{\chi}_i^0} &= \sum_m \left[-\frac{m_\mu}{12m_{\tilde{\chi}_i^0}^2} n_{\mu im}^{L*} n_{eim}^L x_{im} F_1^N(x_{im}) + \frac{1}{3m_{\tilde{\chi}_i^0}} n_{\mu im}^R n_{eim}^L x_{im} F_2^N(x_{im}) \right]. \end{aligned} \quad (3.12)$$

In an obvious analogy to the chargino case, one could introduce $a_{\mu 1,2}^{\tilde{\chi}_i^0}$ etc., but we will not make use of that. In the previous equations, the abbreviations are defined as

$$\begin{aligned} n_{\ell im}^L &= \frac{1}{\sqrt{2}} (g_1 N_{i1} + g_2 N_{i2}) K_{m,\ell}^* - Y_\ell N_{i3} K_{m,\ell+3}^*, \\ n_{\ell im}^R &= \sqrt{2} g_1 N_{i1} K_{m,\ell+3} + Y_\ell N_{i3} K_{m,\ell}, \end{aligned} \quad (3.13)$$

the loop functions are

$$\begin{aligned} F_1^N(x) &= \frac{2}{(1-x)^4} [1 - 6x + 3x^2 + 2x^3 - 6x^2 \ln x], \\ F_2^N(x) &= \frac{3}{(1-x)^3} [1 - x^2 + 2x \ln x], \end{aligned} \quad (3.14)$$

and

$$x_{im} \equiv \frac{m_{\tilde{\chi}_i^0}^2}{m_{\tilde{\ell}_m}^2}. \quad (3.15)$$

To define the slepton masses and mixing we start from the slepton mass terms for the interaction and flavor eigenstates $\tilde{\ell}_{Li}, \tilde{\ell}_{Ri}$ with generation index $i = 1, 2, 3$,

$$(\tilde{\ell}_{L1}^*, \tilde{\ell}_{L2}^*, \dots, \tilde{\ell}_{R3}^*) \mathcal{M}^2 \begin{pmatrix} \tilde{\ell}_{L1} \\ \tilde{\ell}_{L2} \\ \vdots \\ \tilde{\ell}_{R3} \end{pmatrix} = (\tilde{\ell}_{L1}^*, \tilde{\ell}_{L2}^*, \dots, \tilde{\ell}_{R3}^*) \begin{pmatrix} m_L^2 + \mathcal{D}_L^\ell & m_{LR}^{2\dagger} \\ m_{LR}^2 & m_R^2 + \mathcal{D}_R^\ell \end{pmatrix} \begin{pmatrix} \tilde{\ell}_{L1} \\ \tilde{\ell}_{L2} \\ \vdots \\ \tilde{\ell}_{R3} \end{pmatrix} \quad (3.16)$$

with 3×3 block matrices m_L^2 , m_R^2 and $(m_{LR}^2)_{ij} = \delta_{ij} m_i (A_i - \mu^* \tan \beta)$. We have omitted the small F -term contribution m_i^2 involving the lepton masses. We use a basis where the lepton mass matrix is diagonal. The 6×6 mass matrix \mathcal{M}^2 leads to slepton mass eigenvalues $m_{\tilde{\ell}_1} < m_{\tilde{\ell}_2} < \dots < m_{\tilde{\ell}_6}$ and the diagonalization matrix $K_{m\ell}$ defined via

$$K \mathcal{M}^2 K^\dagger = \text{diag}(m_{\tilde{\ell}_1}^2, \dots, m_{\tilde{\ell}_6}^2). \quad (3.17)$$

For the neutralino mass and mixing matrices we use the convention

$$N^* M_{\tilde{\chi}^0} N^{-1} = \text{diag}(m_{\tilde{\chi}_1^0}, \dots, m_{\tilde{\chi}_4^0}). \quad (3.18)$$

4 Correlations in different parameter space regions

4.1 Similar SUSY masses

In order to obtain a first impression of the strength of the correlation between the SUSY contribution

$$a_\mu \equiv \sum_k a_\mu^{\tilde{\chi}_k^\pm} + \sum_i a_\mu^{\tilde{\chi}_i^0} \quad (4.1)$$

and $\text{BR}(\mu \rightarrow e\gamma)$ for generic SUSY spectra without strong mass hierarchies between sleptons, neutralinos and charginos, we perform a random scan over the parameters

$$M_1, M_2, \mu, m_{\tilde{L}_{11}}, m_{\tilde{L}_{22}}, m_{\tilde{R}_{11}}, m_{\tilde{R}_{22}},$$

varying them between 300 GeV and 600 GeV while ensuring that a neutralino is the lightest superparticle (LSP). All other superparticle masses are irrelevant for our calculations. We set the trilinear couplings A_e and A_μ to zero after verifying that they have no impact. We fix $\tan\beta = 50$ and $(\delta_{12}^l)_{LL} = (\delta_{12}^l)_{RR} = 2 \times 10^{-5}$ for the flavor-violating parameters

$$(\delta_{12}^l)_{LL} \equiv \frac{m_{\tilde{L}_{12}}^2}{\sqrt{m_{\tilde{L}_{11}}^2 m_{\tilde{L}_{22}}^2}}, \quad (\delta_{12}^l)_{RR} \equiv \frac{m_{\tilde{R}_{12}}^2}{\sqrt{m_{\tilde{R}_{11}}^2 m_{\tilde{R}_{22}}^2}}. \quad (4.2)$$

The results are shown in figure 1. Taking into account that the correlated quantities are the amplitudes a_μ , $a_{\mu e\gamma L}$ and $a_{\mu e\gamma R}$ whereas $\text{BR}(\mu \rightarrow e\gamma)$ involves amplitudes squared, we observe a correlation that is significant but not extremely strong. This indicates that typically several diagrams contribute, either cancelling each other or adding up constructively. In order to investigate this, we encoded in the color of points the importance of the leading contribution, defined as

$$R \equiv \frac{\max_{i,k} \{|a_\mu^{\tilde{\chi}_k^\pm}|, |a_\mu^{\tilde{\chi}_i^0}|\}}{a_\mu}. \quad (4.3)$$

R is a measure for the degree of cancellation: if a single diagram dominates, $R \approx 1$, while $R > 1$ indicates cancellations; $R < 1$ if diagrams add up constructively. The figure shows that the latter does not occur. In fact, R is larger than about 1.5 for all points. For more than 90% of them we find even $R > 2$. Consequently, significant cancellations are typical.

We have checked that adding the constraints $m_{\tilde{L}_{11}}^2 = m_{\tilde{L}_{22}}^2$ or $m_{\tilde{R}_{11}}^2 = m_{\tilde{R}_{22}}^2$ does not strengthen the correlation significantly. It is also virtually unchanged if we set $(\delta_{12}^l)_{RR} = 0$ while keeping $(\delta_{12}^l)_{LL} = 2 \times 10^{-5}$. On the other hand, the correlation becomes very weak if only $(\delta_{12}^l)_{RR}$ is non-zero. This is to be expected, since only neutralinos contribute to $a_{\mu e\gamma}$ for $(\delta_{12}^l)_{LL} = 0$, whereas a_μ is dominated by charginos for similar SUSY masses. Finally, the correlation is not very sensitive to the value of $\tan\beta$, since the dominant contributions to all amplitudes are proportional to this parameter, so it does not appear in their ratios, see e.g. eq. (3.9). Exceptions can occur for $\tan\beta < 10$, but in this case a_μ is generically too small to be of interest.

In the following we will study scenarios for which the correlation can become stronger. They are characterized by hierarchies within the SUSY spectrum, and table 1 already shows

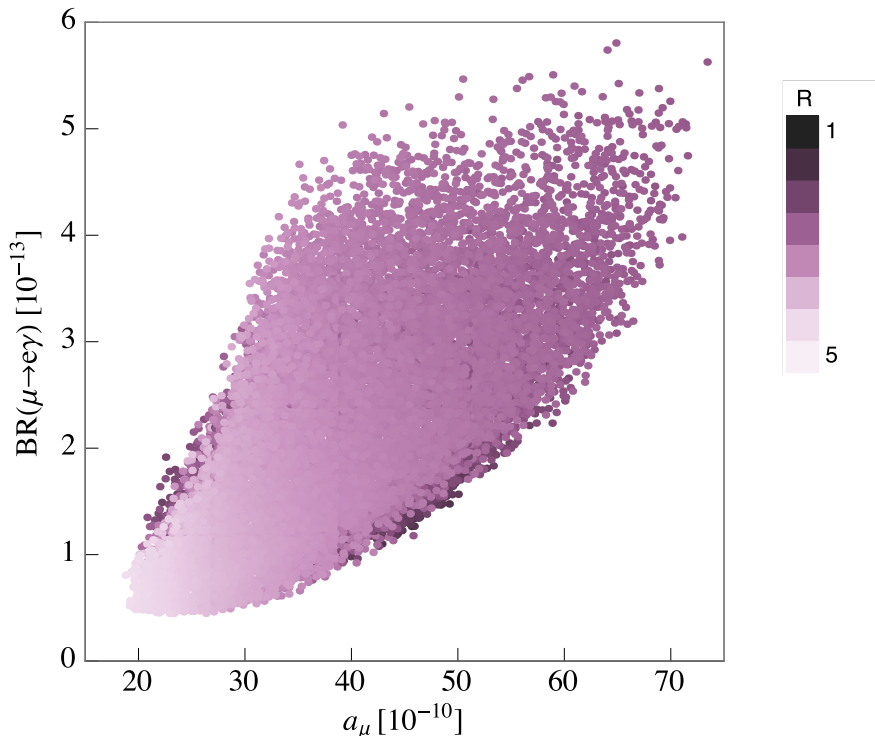


Figure 1. Scatter plot (10^5 points) of a_μ versus $\text{BR}(\mu \rightarrow e\gamma)$ for similar SUSY mass parameters between 300 and 600 GeV, $\tan\beta = 50$, and $(\delta_{12}^l)_{LL} = (\delta_{12}^l)_{RR} = 2 \times 10^{-5}$. The points are color-coded according to the degree of cancellation R , cf. eq. (4.3).

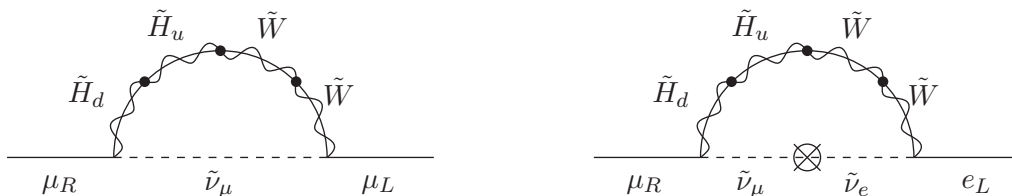


Figure 2. Mass-insertion diagrams involving higgsinos $\tilde{H}_{u,d}$ and winos \tilde{W} , which correspond to the leading contributions to a_μ and $a_{\mu e\gamma}$ in the case of chargino dominance. The external photon can couple to all charged lines. The cross denotes the insertion of the flavor mixing term m_{L12}^2 .

the benchmark parameter choices considered in sections 4.2, 4.3 and 4.4. Comparing these cases with the generic, non-hierarchical case discussed here will further clarify the weak correlation in figure 1. Later, in section 5, we will compare bounds on the flavor-violating parameters for all these cases.

4.2 Chargino dominance

We first focus on cases in which the chargino contributions are dominant. For large $\tan\beta$ they are essentially given by $a_\mu^{\tilde{X}_k^\pm}$ and $a_{\mu e\gamma}^{\tilde{X}_k^\pm}$; the corresponding mass-insertion diagrams

Parameter / Kind of spectrum	II	III	IV
$\tan \beta$	50	50	50
μ	500	150... 5000	-550... -650
M_2	550... 1300	1800	100... 900
M_1	400	320	100
$m_{\tilde{L}_{12}}$	3	2	0
$m_{\tilde{L}_{11}}$	502	470	3001
$m_{\tilde{L}_{22}}$	502	490	3001
$m_{\tilde{R}_{12}}$	0	0	2
$m_{\tilde{R}_{11}}$	900	510	120
$m_{\tilde{R}_{22}}$	950	600	80... 250
$m_{\tilde{\nu}_1}$	496	463	3000
$m_{\tilde{\nu}_2}$	496	483	3000

Table 1. Benchmark parameter choices II (chargino dominance with similar masses, section 4.2), III (large μ , section 4.3), and IV (neutralino- $\tilde{\mu}_R$ dominance, section 4.4). Masses are given in GeV. Numbers printed in gray denote parameters that do not have an important impact on the values of a_μ and $\text{BR}(\mu \rightarrow e\gamma)$ for the respective benchmark. Note that the sneutrino masses are not independent of the other input parameters, and their given values are rounded to integer values.

	Hierarchy	Limiting behavior of $\left \frac{a_{\mu e\gamma}^\pm}{a_\mu^\pm} \right $		Possible realization	LSP constraint
		$I = 1$	$I = 2$		
I	$x_{k1}, x_{k2} \gg 1$	$2 \frac{ m_{\tilde{L}_{12}}^2 }{m_{\tilde{\chi}_k^\pm}^2}$	$\frac{ m_{\tilde{L}_{12}}^2 }{m_{\tilde{\chi}_k^\pm}^2}$	$m_{\tilde{L}_{11}}, m_{\tilde{L}_{22}} \ll M_2, \mu$	
II	$x_{k1}, x_{k2} \ll 1$	$\frac{ m_{\tilde{L}_{12}}^2 }{m_{\tilde{\nu}_1}^2}$	$\frac{ m_{\tilde{L}_{12}}^2 }{ m_{\tilde{\nu}_2}^2 - m_{\tilde{\nu}_1}^2 } \left 1 - \frac{x_{k1} \log x_{k1}}{x_{k2} \log x_{k2}} \right $	$\mu \ll m_{\tilde{L}_{11}}, m_{\tilde{L}_{22}}$	$\mu < m_{\tilde{L}_{11}}$
III	$x_{k1} \ll 1 \ll x_{k2}$	$\frac{ m_{\tilde{L}_{12}}^2 }{m_{\tilde{\nu}_1}^2}$	$\frac{ m_{\tilde{L}_{12}}^2 }{m_{\tilde{\nu}_1}^2}$	$m_{\tilde{L}_{11}} \gg M_2, \mu \gg m_{\tilde{L}_{22}}$	$M_1 < m_{\tilde{L}_{22}}$
IV	$x_{k2} \ll 1 \ll x_{k1}$	$\frac{1}{2} \frac{ m_{\tilde{L}_{12}}^2 }{m_{\tilde{\chi}_k^\pm}^2}$	$\frac{1}{2} \frac{ m_{\tilde{L}_{12}}^2 }{m_{\tilde{\nu}_2}^2} \left 2 + \frac{1}{x_{k2} \log x_{k2}} \right $	$m_{\tilde{L}_{11}} \ll \mu \ll m_{\tilde{L}_{22}}$	
V	$x_{k1} \sim x_{k2} \sim 1$	$\frac{2}{5} \frac{ m_{\tilde{L}_{12}}^2 }{m_{\tilde{\nu}_1}^2}$	$\frac{1}{4} \frac{ m_{\tilde{L}_{12}}^2 }{m_{\tilde{\nu}_2}^2}$	$\mu \sim m_{\tilde{L}_{11}} \sim m_{\tilde{L}_{22}}$	$M_1 < m_{\tilde{L}_{11}}, m_{\tilde{L}_{22}}$
VI	$x_{k1} \sim 1, x_{k2} \gg 1$	$\frac{1}{2} \frac{ m_{\tilde{L}_{12}}^2 }{m_{\tilde{\nu}_1}^2}$	$\frac{1}{3} \frac{ m_{\tilde{L}_{12}}^2 }{m_{\tilde{\nu}_1}^2}$	$\mu \sim m_{\tilde{L}_{11}} \gg m_{\tilde{L}_{22}}$	
VII	$x_{k1} \sim 1, x_{k2} \ll 1$	$\frac{1}{4} \frac{ m_{\tilde{L}_{12}}^2 }{m_{\tilde{\chi}_k^\pm}^2}$	$\frac{1}{3} \frac{ m_{\tilde{L}_{12}}^2 }{m_{\tilde{\chi}_k^\pm}^2} / \log x_{k2}^{-1}$	$\mu \sim m_{\tilde{L}_{11}} \ll m_{\tilde{L}_{22}}$	$\mu < m_{\tilde{L}_{11}}$
VIII	$x_{k2} \sim 1, x_{k1} \gg 1$	$\frac{ m_{\tilde{L}_{12}}^2 }{m_{\tilde{\nu}_2}^2}$	$\frac{1}{2} \frac{ m_{\tilde{L}_{12}}^2 }{m_{\tilde{\nu}_2}^2}$	$m_{\tilde{L}_{11}} \ll \mu \sim m_{\tilde{L}_{22}}$	
IX	$x_{k2} \sim 1, x_{k1} \ll 1$	$\frac{ m_{\tilde{L}_{12}}^2 }{m_{\tilde{\nu}_1}^2}$	$\frac{ m_{\tilde{L}_{12}}^2 }{m_{\tilde{\nu}_1}^2}$	$\mu \sim m_{\tilde{L}_{22}} \ll m_{\tilde{L}_{11}}$	M_2 or $\mu < m_{\tilde{L}_{22}}$

Table 2. Different limits of the ratio $a_{\mu e\gamma}^\pm / a_\mu^\pm$, according to different hierarchies of the parameters x_{ki} , for $I = 1, 2$. These approximations are valid chargino by chargino, thus one may have to consider different hierarchies for the two charginos. The last column shows the constraints to obtain a neutralino LSP; where no constraint is given, this is not possible.

are shown in figure 2. The chargino contributions depend only on four free mass parameters, μ , M_2 , $m_{\tilde{L}_{11}}$, $m_{\tilde{L}_{22}}$, and the mixing $m_{\tilde{L}_{12}}$.

The correlations are governed by eq. (3.10), which relates the contributions to a_μ and $a_{\mu e\gamma L}$ from one individual chargino $\tilde{\chi}_k^\pm$ and has two immediate implications. The ratio $a_{\mu e\gamma L}^{\tilde{\chi}_k^\pm}/a_{\mu}^{\tilde{\chi}_k^\pm}$ in eq. (3.10) depends non-trivially on the mass ratios x_{k1} and x_{k2} ; hence (i) it is different for the two charginos and the correlation between the sums over the contributions can be much weaker than the correlations between the individual contributions, and (ii) even for the individual charginos the right-hand side depends on the mass hierarchy between charginos and sneutrinos.

Table 2 shows a comprehensive list of hierarchies between chargino and sneutrino masses, following ref. [2]. For each hierarchy we analytically evaluated the limiting behavior of the ratio $a_{\mu e\gamma L}^{\tilde{\chi}_k^\pm}/a_{\mu}^{\tilde{\chi}_k^\pm}$. The results are shown in the third and fourth column of the table; they slightly improve similar results of ref. [2]. Note that the result for $I = 2$ is the more relevant one since the $I = 2$ contributions dominate for large $\tan\beta$. The last column shows the conditions that are necessary for having a neutralino LSP. Note that the lightest neutralino need not be the LSP, if a super-weakly interacting particle such as the gravitino or axino is the LSP, or if R parity is violated. Finally, the table also shows mass patterns which realize the hierarchies and which allow dominance of the contributions of the lightest or both charginos over the neutralino contributions. In the following we will study each mass hierarchy, focussing in particular on the deviations from the approximations in the table and on the impact of possible cancellations between individual contributions.

Let us consider first the situation of very similar masses, i.e. case V in table 2,

$$m_{\tilde{L}_{11}} \sim m_{\tilde{L}_{22}} \sim \mu \tag{4.4}$$

or

$$x_{11} \sim x_{12} \sim 1, \tag{4.5}$$

in terms of the mass ratios x_{ki} defined in eq. (3.4). As a concrete example, we choose the parameters appearing in column II of table 1. The chargino masses are driven by μ and M_2 , respectively, $m_{\tilde{\chi}_1^\pm} \approx 500$ GeV and $m_{\tilde{\chi}_2^\pm} \in [550, 1300]$ GeV. The first and second plot of figure 3 show, respectively, the contributions to a_μ and $a_{\mu e\gamma L}$ from each chargino and demonstrate that the lightest chargino provides the dominant contributions. The larger M_2 , the more pronounced the domination becomes. The third plot of the same figure shows the ratios of the contributions from each chargino individually and the ratio of the sums of all contributions to a_μ and $a_{\mu e\gamma L}$. The ratios are compared with the prediction for the theoretical limiting behavior given in table 2, $|a_{\mu e\gamma L}/a_\mu| = \frac{1}{4} \frac{|m_{L12}^2|}{m_{\tilde{\nu}_2}^2}$. Indeed, the ratio for the lightest chargino agrees excellently with this prediction, because the hierarchy condition $x_{11} \sim x_{12} \sim 1$ is satisfied precisely. For the heaviest chargino, x_{21} and x_{22} are significantly larger than 1, except at the lower end of the considered interval for M_2 , so for higher M_2 the corresponding ratio deviates more and more from $\frac{1}{4} \frac{|m_{L12}^2|}{m_{\tilde{\nu}_2}^2}$. Due to the dominance of the lightest chargino, the ratio of the sum of all contributions agrees with the prediction within a factor 1.5 for all values of M_2 shown in the plot. The absolute value of this

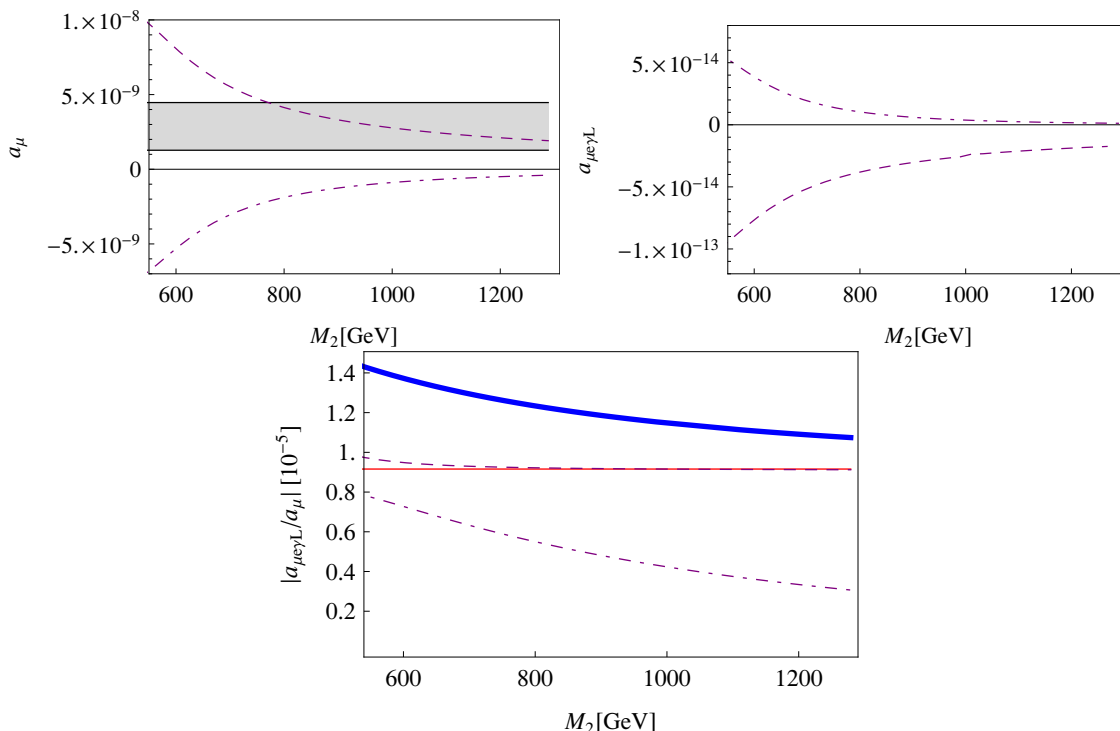


Figure 3. a_μ , $a_{\mu e\gamma L}$ and their ratio as a function of M_2 for the parameters in column II of table 1, equivalently case V in eq. (4.6) and table 2. Top: contributions to a_μ and $a_{\mu e\gamma L}$ from each individual chargino. The long-dashed (dot-dashed) curve corresponds to the lightest (heaviest) chargino. The shaded area marks the favored 2σ region according to eq. (2.1). Bottom: the ratio $|a_{\mu e\gamma L}^{\tilde{\chi}_k^\pm}/a_\mu^{\tilde{\chi}_k^\pm}|$ for each chargino (same line styles as in the top row). For comparison, the corresponding approximation for $|a_{\mu e\gamma}^{\tilde{\chi}_k^\pm}/a_\mu^{\tilde{\chi}_k^\pm}|$, case V in table 2, is shown as a thin solid red line. The total ratio including neutralino contributions, $|a_{\mu e\gamma L}/a_\mu|$, is shown as the thick solid blue line.

ratio, $|a_{\mu e\gamma L}/a_\mu|$, is larger than both individual ratios $|a_{\mu e\gamma L}^{\tilde{\chi}_k^\pm}/a_\mu^{\tilde{\chi}_k^\pm}|$, which indicates that the cancellation between the different contributions is stronger for a_μ than for $a_{\mu e\gamma L}$. As M_1 is the smallest of the soft SUSY breaking parameters, the LSP is a neutralino with dominant bino component.

We will now study systematically all nine cases listed in table 2. We set the mass parameters to definite values according to the hierarchies given in the table, but such that the lightest chargino still represents the leading contribution to a_μ , and such that the value of a_μ remains inside the region allowed by eq. (2.1). We use the following sets of parameters:

- I. $m_{\tilde{\nu}_e} = 127$ GeV, $m_{\tilde{\nu}_\mu} = 117$ GeV, $\mu = 550$ GeV, $M_1 = 700$ GeV,
- II. $m_{\tilde{\nu}_e} = 489$ GeV, $m_{\tilde{\nu}_\mu} = 693$ GeV, $\mu = 220$ GeV, $M_1 = 700$ GeV,
- III. $m_{\tilde{\nu}_e} = 3500$ GeV, $m_{\tilde{\nu}_\mu} = 356$ GeV, $\mu = 1400$ GeV, $M_1 = 350$ GeV,
- IV. $m_{\tilde{\nu}_e} = 96$ GeV, $m_{\tilde{\nu}_\mu} = 965$ GeV, $\mu = 320$ GeV, $M_1 = 400$ GeV,
- V. $m_{\tilde{\nu}_e} = 496$ GeV, $m_{\tilde{\nu}_\mu} = 496$ GeV, $\mu = 500$ GeV, $M_1 = 400$ GeV, (4.6)

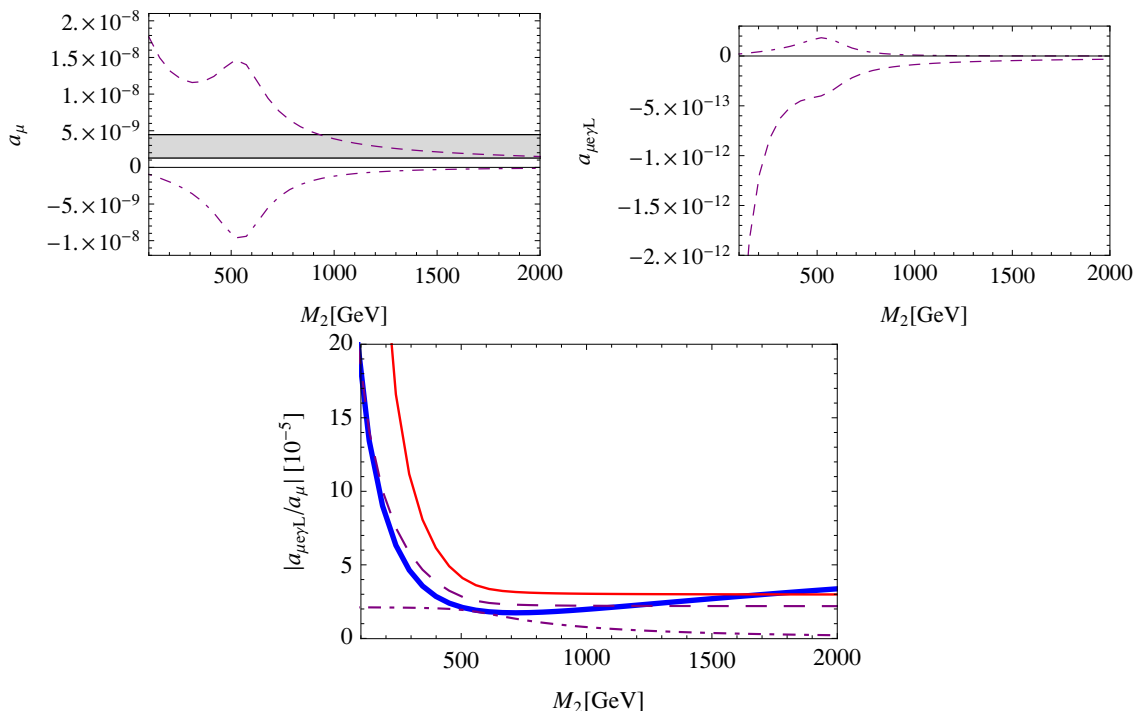


Figure 4. Case I. Same as in figure 3, but for case I in table 2 and eq. (4.6). The thin solid red line corresponds to the approximation for the lightest chargino, $k = 1$.

- | | | | | |
|-------|---|--|--------------------------|--------------------------|
| VI. | $m_{\tilde{\nu}_e} = 797 \text{ GeV},$ | $m_{\tilde{\nu}_\mu} = 131 \text{ GeV},$ | $\mu = 800 \text{ GeV},$ | $M_1 = 700 \text{ GeV},$ |
| VII. | $m_{\tilde{\nu}_e} = 256 \text{ GeV},$ | $m_{\tilde{\nu}_\mu} = 917 \text{ GeV}$ | $\mu = 260 \text{ GeV},$ | $M_1 = 500 \text{ GeV},$ |
| VIII. | $m_{\tilde{\nu}_e} = 66 \text{ GeV},$ | $m_{\tilde{\nu}_\mu} = 550 \text{ GeV}$ | $\mu = 550 \text{ GeV},$ | $M_1 = 500 \text{ GeV},$ |
| IX. | $m_{\tilde{\nu}_e} = 1738 \text{ GeV},$ | $m_{\tilde{\nu}_\mu} = 520 \text{ GeV},$ | $\mu = 500 \text{ GeV},$ | $M_1 = 900 \text{ GeV}.$ |

Here we have used $m_{\tilde{\nu}_e}^2 \equiv m_{L_{11}}^2 + \mathcal{D}_L^\nu$ and $m_{\tilde{\nu}_\mu}^2 \equiv m_{L_{22}}^2 + \mathcal{D}_L^\nu$ as more physical inputs. In addition, $\tan \beta = 50$, $m_{L_{12}}^2 = (3 \text{ GeV})^2$, and the value of M_2 is kept as a variable.

For each case, we focus on the following questions: does the limiting behavior in table 2 provide a reliable prediction for the correlation between a_μ and $a_{\mu e \gamma}$ for (i) the individual contribution of the lighter chargino and (ii) the sum of all contributions? We consider the prediction reliable if it agrees with the precise numerical result up to a factor of 1.5 or less. In addition, (iii) are the scenarios compatible with a neutralino LSP? We will be briefer in our discussions than for case V discussed above, but we will highlight cases I, VI, and VII, each of which illustrates a different behavior. Case V is an example where all three criteria are met. In case VI, (i) and (ii) are satisfied but (iii) is not. Case I is an example where (i) is satisfied whereas (ii) is met only in a part of the considered mass range for M_2 . Case VII is an example where only (i) and (iii) are satisfied; in addition, the approximation to $a_{\mu e \gamma}^{\tilde{\chi}_k^\pm} / a_\mu^{\tilde{\chi}_k^\pm}$ cannot be written as a ratio of two parameters, because there are logarithmic contributions that become relevant. For these cases we also show plots analogous to figure 3, see figures 4–6.

- For case I, both μ and M_2 must be considerably bigger than the sneutrino masses to generate the hierarchy $x_{k1}, x_{k2} \gg 1$, which pushes the masses of both charginos and three neutralinos well above the masses of the sneutrinos. In order to guarantee chargino dominance, we also set M_1 to a high value, which implies that in case I we cannot obtain a neutralino LSP. Figure 4 shows that the approximation for the ratio $a_{\mu e \gamma}^{\tilde{\chi}_k^\pm} / a_{\mu}^{\tilde{\chi}_k^\pm}$ works within 50% accuracy for the lightest chargino. It fails in the low- M_2 region where x_{1i} becomes smaller than about 8, since there the expansion of the ratio in eq. (3.9) is not valid anymore. As it depends on the chargino mass, the approximation for $k = 1$ plotted in the figure cannot describe the contribution of the heavier chargino. Besides, at $\mu = M_2$ the chargino mixing becomes maximal, and so does the cancellation between the chargino contributions. Hence, approximating one of them well can be meaningless for the sum. The approximation works reliably for the sum only for $M_2 \gtrsim 1$ TeV.
- For case II, the approximation in table 2 contains a factor involving logarithms. This factor can change the result by more than a factor of 2 and therefore should not be neglected. If it is included, the approximation works very well for the contribution of the lighter chargino and satisfactorily for the sum. For the specific example in eq. (4.6) and $M_2 \gg \mu$, the LSP is a higgsino-like neutralino with a mass around 216 GeV.
- For case III the approximation works quite well for the sum and for the contribution of the lighter chargino for all values of M_2 up to about 1 TeV. It is no problem to consider relatively small values of M_1 , so the LSP can be a bino-like neutralino. For the values quoted in eq. (4.6), the LSP has a mass around 350 GeV.
- Case IV interchanges the roles of $\tilde{\nu}_e$ and $\tilde{\nu}_\mu$ compared to case III. Due to the higher $m_{\tilde{\nu}_\mu}$ the contribution to both observables is suppressed, and the approximation for the ratio $a_{\mu e \gamma L} / a_\mu$ depends in a complicated way on the chargino and $\tilde{\nu}_\mu$ masses. We find that even the full approximation shown in table 2 does not work reliably. The hierarchy required in case IV forbids very light values of μ and M_2 around 100 GeV, and the requirement of chargino dominance forbids values of M_1 smaller than around 400 GeV. This case thus does not allow a neutralino LSP.
- For case V, see the discussion above.
- For case VI, both μ and M_2 must be kept large to generate the hierarchies $x_{k2} \gg 1$, $x_{k1} \sim 1$. If this is satisfied, the approximation works well for the lighter chargino. It also provides a reliable prediction for the sum of the contributions with about 40% accuracy for all values $M_2 > 800$ GeV, see figure 5. The bino mass should be heavy, $M_1 \gtrsim 500$ GeV, to avoid neutralino contributions to be dominant, so with the hierarchy of this case it is not possible to obtain a neutralino LSP.
- Case VII is shown in figure 6. The plotted range for M_2 is the one where a_μ is within the favored 2σ region. The μ parameter is small enough to satisfy the LSP condition

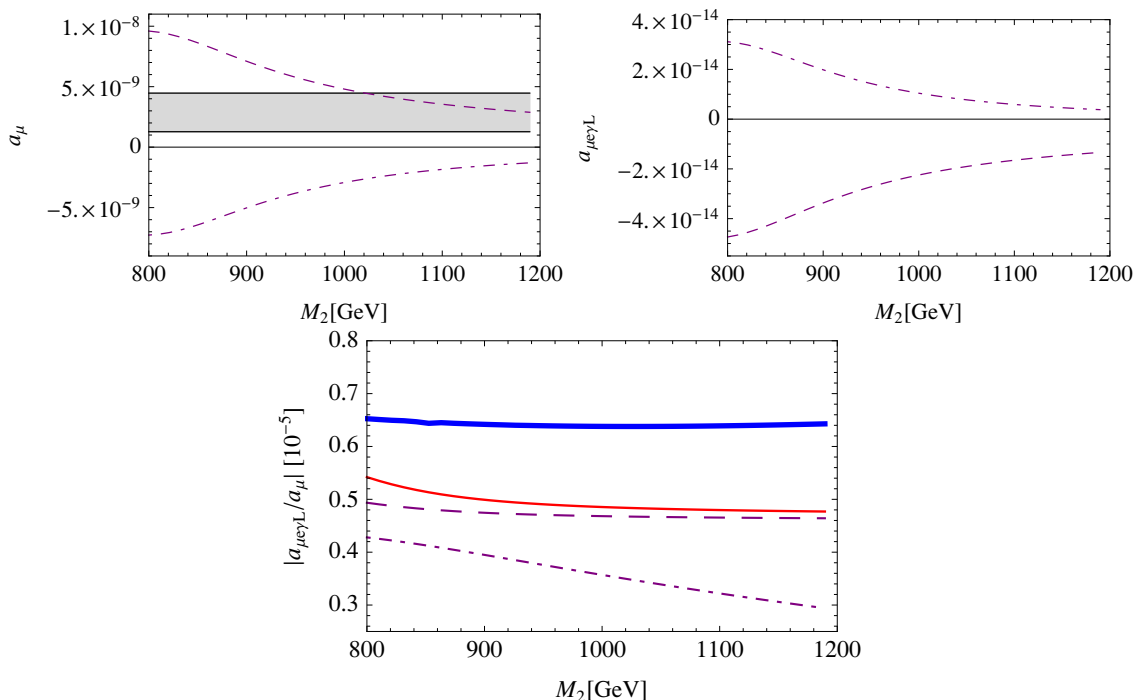


Figure 5. Case VI. Same as in figure 3, but for case VI in table 2 and eq. (4.6).

$m_{\tilde{\chi}_1^0} < m_{\tilde{\nu}_1}$. In this case it is important not to neglect the logarithmic factor in the approximation for $a_{\mu e \gamma}^{\tilde{\chi}_k^\pm} / a_{\mu}^{\tilde{\chi}_k^\pm}$, which then works very well for the lightest chargino. However, interestingly the sum of the contributions is not sufficiently dominated by the lightest chargino, so the approximation fails to predict the ratio $a_{\mu e \gamma L} / a_{\mu}$ correctly.

- Case VIII is similar to case VI in that both μ and M_2 must be kept large to generate the hierarchies, which together with the requirement of subdominant neutralino contributions makes it impossible to obtain a neutralino LSP. The approximation for $a_{\mu e \gamma}^{\tilde{\chi}_k^\pm} / a_{\mu}^{\tilde{\chi}_k^\pm}$ works well for the contribution of the lightest chargino but not for the sum, which shows a strong dependence on M_2 .
- For case IX, the approximation of the ninth line in table 2 works quite well for both the lightest chargino contribution and for the sum of the contributions from the two charginos. In this case it is possible to obtain a neutralino LSP. For the example of eq. (4.6), it could be higgsino- or wino-like, depending on the value of M_2 in comparison to μ , which remains fixed at 500 GeV.

Note that for all these cases the values of $m_{\tilde{R}_{11}}$ and $m_{\tilde{R}_{22}}$ are not important. These parameters just have to be sufficiently large to avoid the appearance of a charged LSP.

In summary, depending on the hierarchy of the sneutrino and chargino masses, the different approximations to $a_{\mu e \gamma}^{\tilde{\chi}_k^\pm} / a_{\mu}^{\tilde{\chi}_k^\pm}$ given in table 2 predict the ratio of the lighter

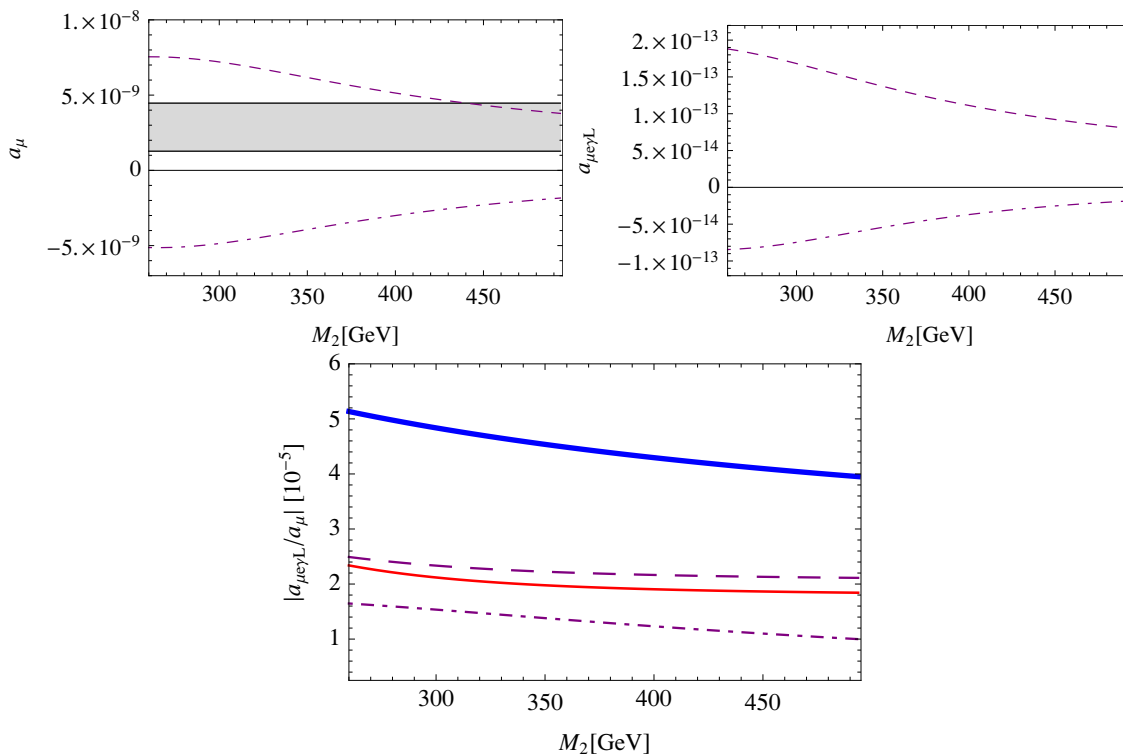


Figure 6. Case VII. The same as in figure 3, but for case VII in table 2 and eq. (4.6).

chargino’s contributions to $a_{\mu e \gamma L}$ and a_μ reliably, i.e. within a factor 1.5 of accuracy, with case IV being the sole exception. In cases I (for $M_2 \gtrsim 1$ TeV), II, III, V, VI, and IX, these approximations can also be used as a reliable substitute for the exact value of $a_{\mu e \gamma L} / a_\mu$ stemming from all contributions. However, in case II the approximation depends on three superparticle masses, weakening the link between the two observables. In the remaining cases I, III, V, VI, and IX, there is a strong correlation; we can predict $\text{BR}(\mu \rightarrow e \gamma)$ as a function of a_μ and the ratio of the flavor-violating parameter and a single superpartner mass within a factor of roughly 1.5^2 .

Figure 7 summarizes the present section and allows further interpretation of the similar-mass case of the previous section 4.1. It shows $\text{BR}(\mu \rightarrow e \gamma)$ versus a_μ for the benchmark points listed in eq. (4.6) and for random SUSY masses. The scatter regions repeat the similar-mass case of figure 1, but this time focussing on the effect of different mass intervals instead of the strength of cancellation. The random SUSY masses are generated in the regions [430, 530] GeV (dark blue region), [300, 600] GeV (light blue) and [200, 1000] GeV (yellow). We have fixed $(\delta_{12}^l)_{LL} = (\delta_{12}^l)_{RR} = 2 \times 10^{-5}$.

The benchmark points represent parameter choices with certain extreme mass hierarchies, each of which leads to a different correlation between $\text{BR}(\mu \rightarrow e \gamma)$ and a_μ , as we have discussed in this section. Indeed, one finds a wide variety of branching ratios even for almost the same values of a_μ , see e.g. dots 2, 5, and 6, which are nearly aligned on a common vertical line.

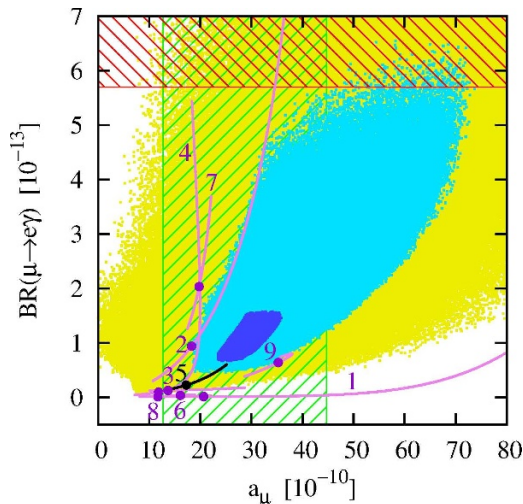


Figure 7. Comparison of our chargino dominance benchmark points to the general scatter plots of $\text{BR}(\mu \rightarrow e\gamma)$ versus a_μ . The numbered dots correspond to the benchmark points listed in eq. (4.6), with M_2 chosen as the midpoint of the ranges shown in figures 3–6. The curves arise from the variation of M_2 within these ranges. For cases II–IV, $M_2 \in [100, 1500]$ GeV, for case VIII, $M_2 \in [550, 2050]$ GeV, and for case IX, $M_2 \in [80, 400]$ GeV. The hatched vertical band depicts the 2σ range of Δa_μ , and the hatched top region is excluded at the 90% C.L. by MEG. For the general scatter plots we have fixed $(\delta_{12}^l)_{LL} = (\delta_{12}^l)_{RR} = 2 \times 10^{-5}$ and selected SUSY masses in the regions [430, 530] GeV (dark blue), [300, 600] GeV (light blue) and [200, 1000] GeV (yellow).

Given those drastically different limits of the ratio, the reason becomes transparent for the wide spread of the points in the scatter regions, where the masses are similar but not exactly equal.

4.3 Large μ limit

If $\tan\beta$ is large, an interesting neutralino contribution to a_μ and $a_{\mu e\gamma}$ is represented by the mass-insertion diagrams in figure 8 with bino exchange. These diagrams grow linearly with μ . Their contribution to a_μ is proportional to $m_\mu^2 \mu \tan\beta M_1 F(M_1, m_{\tilde{\mu}_R}, m_{\tilde{\mu}_L})$, where F denotes the loop function involved in each diagram. All other contributions involve higgsinos and are therefore suppressed for large μ . Hence, the diagrams of figure 8 dominate for sufficiently large μ . We now analyze this parameter region and the behavior of a_μ and $a_{\mu e\gamma}$. Very recently, a_μ in this scenario has also been studied in detail in ref. [26]. The most important parameters of the parameter region with large μ are $\mu, M_1, m_{L22}^2, m_{R22}^2$ and $\tan\beta$. For our analysis we choose $\tan\beta = 50$ and keep all supersymmetric mass parameters except μ and M_2 between 200 and 600 GeV. We vary μ , focussing on the region where

$$\mu > M_2 > M_1. \tag{4.7}$$

Choosing M_2 significantly larger than M_1 further increases the dominance of the contribution of the lightest neutralino for large μ .

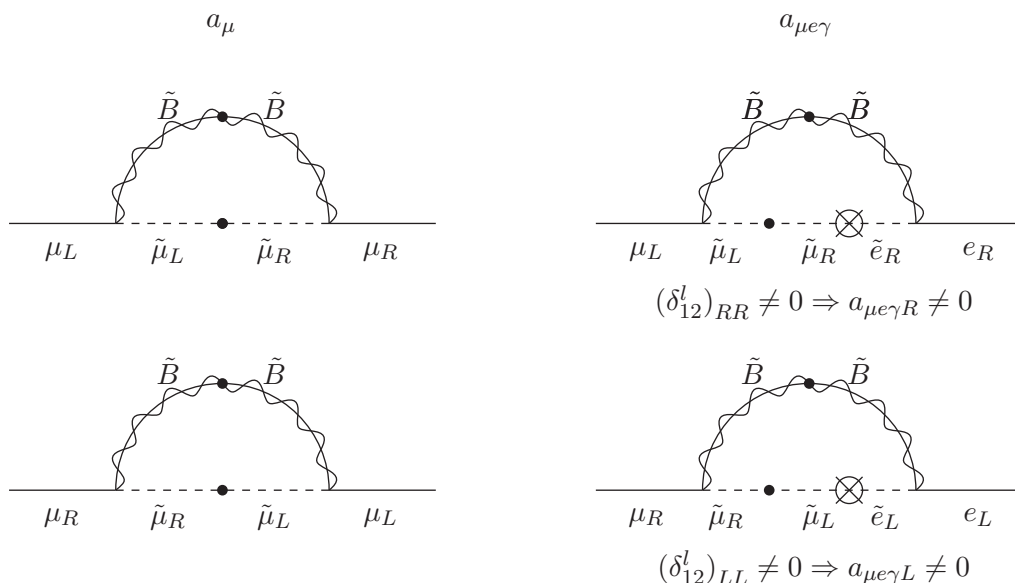


Figure 8. Leading contributions to a_μ and $a_{\mu e\gamma}$ in the case of large μ .

Note that for large values of μ and $\tan\beta$, charge-breaking minima in the scalar potential endanger the stability of the electroweak vacuum. This problem can be alleviated by increasing the stau masses [26], which otherwise have no impact on a_μ and $a_{\mu e\gamma}$.

Interplay of contributions to a_μ . In figure 9, we present an example for this scenario and show a_μ as a function of μ for the parameter choice of spectrum III in table 1. The thick solid (orange) curve corresponds to the total SUSY contribution to a_μ . The solid black line corresponds to the total neutralino contribution and the dot-dashed black line to the contribution of the lightest (bino-like) neutralino. As we can see this lightest neutralino almost fully accounts for the total a_μ in the large- μ region, where μ is significantly larger than M_2 . Here the diagrams of figure 8 dominate. We have also plotted the other individual neutralino contributions (as blue solid, dotted, and dashed lines) and extended the figure down to smaller values of μ , so that it shows the transition from a regime with chargino dominance at low μ to the bino-dominated regime. At very small values of μ , the chargino contributions are important and the neutralino contributions only account for a fraction of the total a_μ . At intermediate values, for $\mu \approx M_1$ or $\mu \approx M_2$, there are two neutralino mass eigenstates whose contributions are strongly enhanced due to large neutralino mixing. However, the enhanced contributions roughly cancel each other, so the sum of all contributions shows no enhancement. This can be understood from the mass-insertion diagrams, which have a monotonous behavior. Around $\mu \approx 500$ GeV, we notice a discontinuity in the plot, which reflects an exchange of identity of the higgsino-like mass eigenstates $\tilde{\chi}_2^0$ and $\tilde{\chi}_3^0$ that is caused by the mixing between higgsinos and gauginos.

In the large μ limit, the total SUSY contribution can be written as

$$a_\mu \approx g_1^2 \frac{m_\mu}{48\pi^2} \sum_m \text{Re}[K_{m5}^* K_{m2}] \frac{M_1}{m_{\tilde{\ell}_m}^2} F_2^N(x_{1m}), \quad (4.8)$$

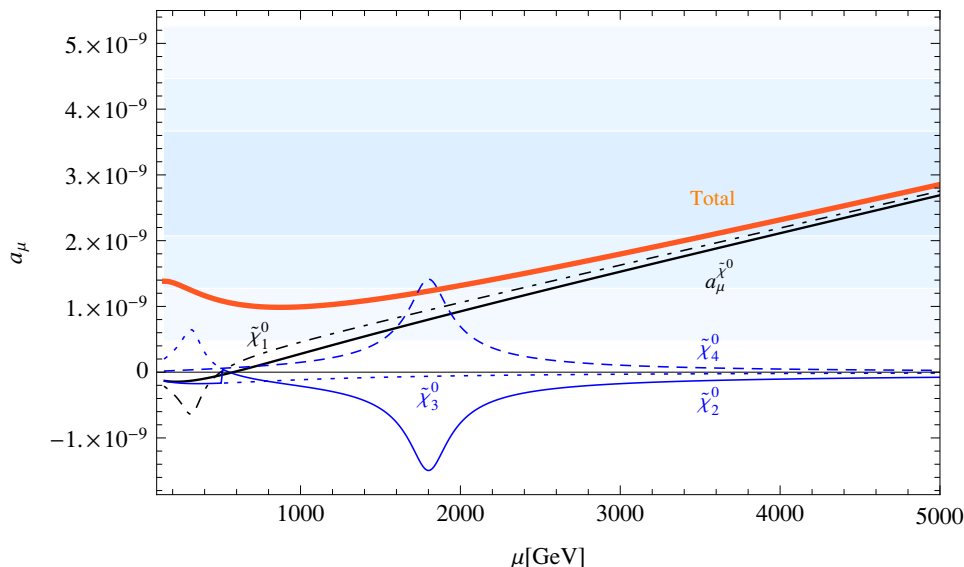


Figure 9. a_μ as a function of μ for the large- μ case of spectrum III in table 1. The thick solid (orange) curve corresponds to the total SUSY contribution. The solid black line corresponds to the total neutralino contribution, and the dot-dashed black line to the contribution of the lightest, bino-like neutralino, which is dominant for large μ . The contributions of the other neutralinos are shown as blue lines. The horizontal bands represent the experimentally allowed regions at 1σ , 2σ and 3σ , respectively.

where x_{1m} is defined in eq. (3.15). As long as flavor violation is small, the most important contributions to a_μ come from the two mass eigenstates containing mainly $\tilde{\mu}_L$ and $\tilde{\mu}_R$, which we label as $m = b$ and $m = c$. Then a_μ can be very well approximated by

$$a_\mu \approx g_1^2 \frac{m_\mu}{48\pi^2} \frac{1}{M_1} \{ \text{Re}[K_{b5}^* K_{b2}] x_{1b} F_2^N(x_{1b}) + \text{Re}[K_{c5}^* K_{c2}] x_{1c} F_2^N(x_{1c}) \}. \quad (4.9)$$

The factors $K_{m5}^* K_{m2}$ determine the mixing between $\tilde{\mu}_L$ and $\tilde{\mu}_R$, which is a necessary ingredient as shown by figure 8. As we are dealing with the mixing of only two states, we can introduce a mixing angle $\theta_{\tilde{\mu}}$ with

$$K_{b5} K_{b2} \approx -K_{c5} K_{c2} \approx \frac{1}{2} \sin 2\theta_{\tilde{\mu}} = \frac{(m_{LR}^2)_{22}}{m_{\tilde{\ell}_b}^2 - m_{\tilde{\ell}_c}^2} \quad (4.10)$$

in analogy to eq. (3.5), where we have restricted ourselves to real parameters and chosen the states such that $m_{\tilde{\ell}_b} < m_{\tilde{\ell}_c}$. We can safely neglect the trilinear coupling in the smuon mixing term $(m_{LR}^2)_{22} = m_\mu (A_\mu - \mu^* \tan \beta)$ and retain only $\mu \tan \beta$. Then we can write a_μ as

$$a_\mu \approx g_1^2 \frac{m_\mu^2}{48\pi^2} \frac{\mu \tan \beta}{M_1} \frac{x_{1b} F_2^N(x_{1b}) - x_{1c} F_2^N(x_{1c})}{m_{\tilde{\ell}_c}^2 - m_{\tilde{\ell}_b}^2}. \quad (4.11)$$

For not too hierarchical smuon masses, the contributions from the two mass eigenstates are of the same order and partially cancel. Note that $x F_2^N(x)$ increases monotonously, so

$a_\mu > 0$ for $\mu > 0$. The result for this scenario can be summarized as

$$a_\mu \approx 2 \times 10^{-9} \left(\frac{\mu}{4 \text{ TeV}} \right) \left(\frac{\tan \beta}{50} \right) \left(\frac{300 \text{ GeV}}{M_1} \right) \left(\frac{1 \text{ TeV}}{m_{\tilde{\ell}_c} + m_{\tilde{\ell}_b}} \right) \left(\frac{100 \text{ GeV}}{m_{\tilde{\ell}_c} - m_{\tilde{\ell}_b}} \right) \left(\frac{\Delta(xF_2^N)}{0.1} \right),$$

$$\Delta(xF_2^N) \equiv x_{1b}F_2^N(x_{1b}) - x_{1c}F_2^N(x_{1c}). \quad (4.12)$$

We could further approximate

$$\frac{\Delta(xF_2^N)}{m_{\tilde{\ell}_c}^2 - m_{\tilde{\ell}_b}^2} \approx \frac{M_1^2}{m_{\tilde{\ell}_b}^2 m_{\tilde{\ell}_c}^2} \frac{d}{dx} xF_2^N(x) \Big|_{x_{1a}}, \quad (4.13)$$

where the numerical value of the derivative varies slowly around 1 in the region of interest. Thus, increasing M_1 increases a_μ if all other parameters are kept fixed.

Interplay of contributions to $a_{\mu e \gamma}$. We consider small flavor-violating terms $m_{\tilde{L}_{12}}^2$ and $m_{\tilde{R}_{12}}^2$,

$$\frac{m_{\tilde{L}_{12}}^2}{m_{\tilde{L}_{22}}^2} \ll 1, \quad \frac{m_{\tilde{R}_{12}}^2}{m_{\tilde{R}_{22}}^2} \ll 1. \quad (4.14)$$

For large μ , we have then

$$a_{\mu e \gamma L} \approx g_1^2 \frac{m_\mu}{48\pi^2} \sum_m K_{m1}^* K_{m5} \frac{M_1}{m_{\tilde{\ell}_m}^2} F_2^N(x_{1m}), \quad (4.15)$$

$$a_{\mu e \gamma R} \approx g_1^2 \frac{m_\mu}{48\pi^2} \sum_m K_{m4}^* K_{m2} \frac{M_1}{m_{\tilde{\ell}_m}^2} F_2^N(x_{1m}). \quad (4.16)$$

Let us first study the case $m_{\tilde{R}_{12}}^2 = 0$ and $m_{\tilde{L}_{12}}^2 \neq 0$, which implies that only $a_{\mu e \gamma L}$ is non-negligible. As we can see from the corresponding diagram in figure 8, $a_{\mu e \gamma L}$ receives contributions from the three mass eigenstates containing mainly \tilde{e}_L , $\tilde{\mu}_L$ and $\tilde{\mu}_R$.¹ Let us denote them by $\tilde{\ell}_a$, $\tilde{\ell}_b$ and $\tilde{\ell}_c$, respectively. For these states we estimate

$$K_{a1}K_{a5} \approx \theta_{\tilde{\mu}} \left(\frac{m_{\tilde{L}_{12}}^2}{m_{\tilde{\ell}_c}^2 - m_{\tilde{\ell}_a}^2} - \frac{m_{\tilde{L}_{12}}^2}{m_{\tilde{\ell}_b}^2 - m_{\tilde{\ell}_a}^2} \right), \quad (4.17)$$

$$K_{b1}K_{b5} \approx \theta_{\tilde{\mu}} \frac{m_{\tilde{L}_{12}}^2}{m_{\tilde{\ell}_b}^2 - m_{\tilde{\ell}_a}^2}, \quad (4.18)$$

$$K_{c1}K_{c5} \approx -\theta_{\tilde{\mu}} \frac{m_{\tilde{L}_{12}}^2}{m_{\tilde{\ell}_c}^2 - m_{\tilde{\ell}_a}^2}, \quad (4.19)$$

assuming real parameters and that all mixings between selectrons and smuons are small. Plugging these expressions into eq. (4.15) yields

$$a_{\mu e \gamma L} \approx g_1^2 \frac{m_\mu^2}{48\pi^2} \frac{\mu \tan \beta}{M_1} \frac{m_{\tilde{L}_{12}}^2}{m_{\tilde{\ell}_c}^2 - m_{\tilde{\ell}_b}^2} \left[\frac{x_{1a}F_2^N(x_{1a}) - x_{1c}F_2^N(x_{1c})}{m_{\tilde{\ell}_c}^2 - m_{\tilde{\ell}_a}^2} - \frac{x_{1a}F_2^N(x_{1a}) - x_{1b}F_2^N(x_{1b})}{m_{\tilde{\ell}_b}^2 - m_{\tilde{\ell}_a}^2} \right]. \quad (4.20)$$

¹If there was a large flavor-violating entry in $m_{\tilde{L}R}^2$, two eigenstates (those containing mainly $\tilde{\mu}_R$ and \tilde{e}_L) could dominate.

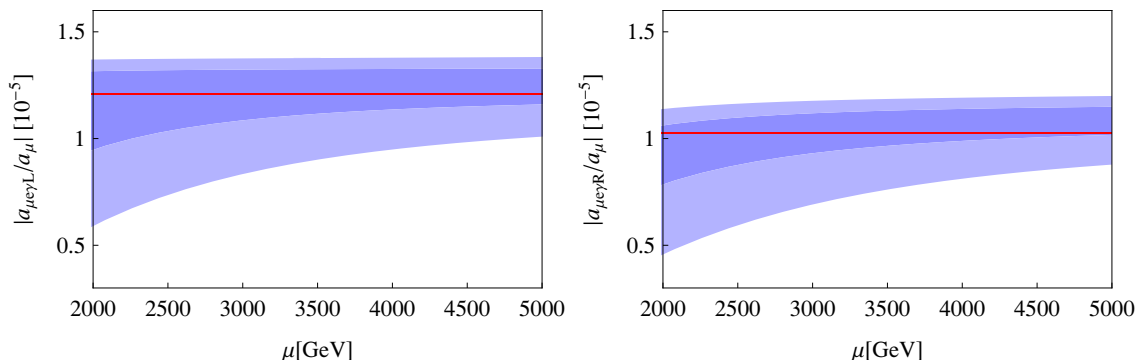


Figure 10. Correlation for the case of large μ , for a range of slepton masses. Left: $|a_{\mu e \gamma L} / a_\mu|$ with $m_{\tilde{L}_{12}} = 2 \text{ GeV}$, $m_{\tilde{R}_{12}} = 0$, $m_{\tilde{L}_{11}} = 470 \text{ GeV}$, and all other slepton masses varied. The remaining parameters were set to the values given in column III of table 1. Right: the same but left- and right-handed parameters exchanged, and $m_{\tilde{R}_{11}}$ fixed to 510 GeV. The light-blue shaded areas correspond to the range [200, 900] GeV, the dark-blue shaded areas to [300, 600] GeV, and the red lines to the approximations of eq. (4.21) and eq. (4.22), respectively.

The ratio $a_{\mu e \gamma L} / a_\mu$ is now easily obtained from eqs. (4.11) and (4.20). We find that this ratio can be well approximated by the numerical estimate

$$\left| \frac{a_{\mu e \gamma L}}{a_\mu} \right| \approx \frac{2}{3} \frac{|m_{\tilde{L}_{12}}^2|}{m_{\tilde{\ell}_a}^2}, \tag{4.21}$$

if all slepton masses are below a TeV. For masses between 300 GeV and 600 GeV, it deviates from the exact result by less than 30%, while for the wider mass range [200, 900] GeV the difference can be up to a factor of 2. The first plot of figure 10 demonstrates that the approximation is even more accurate if we fix $m_{\tilde{L}_{11}}^2 = 470 \text{ GeV}$ and vary only the other slepton masses. Note that the points in the figure correspond to mass differences $|m_{\tilde{\ell}_b} - m_{\tilde{\ell}_c}| \gtrsim 1 \text{ GeV}$, which is generically expected due to the difference between the D -terms of $\tilde{\mu}_L$ and $\tilde{\mu}_R$. Fine-tuning the mass eigenvalues could lead to extreme cancellations and thus to points outside the colored regions in figure 10. When $m_{\tilde{R}_{12}}^2 \neq 0$ and $m_{\tilde{L}_{12}}^2 = 0$, we can proceed in an analogous way, and we find

$$\left| \frac{a_{\mu e \gamma R}}{a_\mu} \right| \approx \frac{2}{3} \frac{|m_{\tilde{R}_{12}}^2|}{m_{\tilde{\ell}_a}^2}. \tag{4.22}$$

This approximation is compared to the exact result in the second plot of figure 10, this time fixing $m_{\tilde{R}_{11}}^2 = 510 \text{ GeV}$. In both plots of figure 10 the solid (red) lines represent the approximations (4.21) and (4.22), while the shaded (blue) areas originate from the random variation of parameters.

4.4 Neutralino- $\tilde{\mu}_R$ dominance

We consider the contributions from the diagrams of figure 11, which involve the right-handed smuon $\tilde{\mu}_R$. They dominate if the spectrum satisfies

$$M_1, m_{\tilde{\mu}_R}, m_{\tilde{e}_R} < M_2, |\mu| \ll m_{\tilde{\mu}_L}, m_{\tilde{e}_L}, \tag{4.23}$$

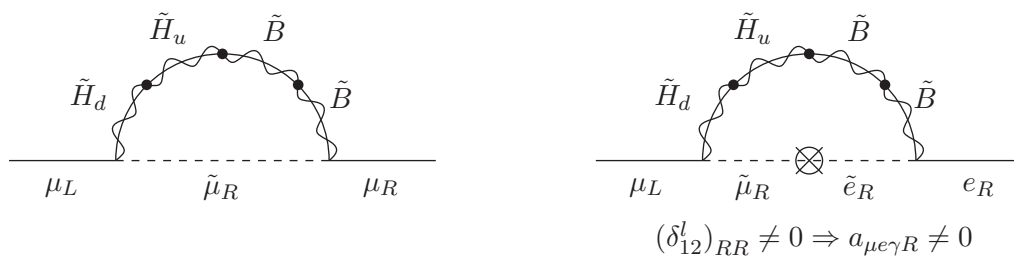


Figure 11. Diagrams corresponding to the leading contributions to a_μ and $a_{\mu e\gamma R}$ in the case of $\tilde{\mu}_R$ dominance.

where the hierarchy $M_1 < M_2, |\mu|$ ensures a bino-like lightest neutralino. Note that $\mu < 0$ in order to have a positive a_μ [25, 27]. The contributions from the diagrams of figures 2 and 8 are suppressed due to the large values of the left-handed slepton masses.

Interplay of contributions to a_μ . From the left diagram of figure 11 we can then estimate a_μ as²

$$\begin{aligned}
 a_\mu &\approx -g_1 g_2 \frac{m_\mu^2}{48\pi^2 M_W \cos\beta} \frac{1}{M_1} \text{Re}[N_{11} N_{13}] x_{1a} F_2^N(x_{1a}) \\
 &\approx -g_1^2 \frac{m_\mu^2 \tan\beta}{48\pi^2 M_1 \mu} x_{1a} F_2^N(x_{1a}),
 \end{aligned} \tag{4.24}$$

where we have labeled the state which is mostly $\tilde{\mu}_R$ as $\tilde{\ell}_a$. Numerically, we can summarize the behavior of a_μ for this case as

$$a_\mu \approx 3 \times 10^{-9} x_{1a} F_2^N(x_{1a}) \left(\frac{\tan\beta}{50}\right) \left(\frac{500 \text{ GeV}}{-\mu}\right) \left(\frac{100 \text{ GeV}}{M_1}\right). \tag{4.25}$$

For the set of parameters in column IV of table 1, the $\tilde{\chi}^0 - \tilde{\mu}_R$ contribution dominates and the value of a_μ is within the allowed 1σ region if $m_{\tilde{\mu}_R} \lesssim 90 \text{ GeV}$, within the 2σ region if $m_{\tilde{\mu}_R} \lesssim 130 \text{ GeV}$ and within the 3σ region if $m_{\tilde{\mu}_R} \lesssim 220 \text{ GeV}$. A benchmark parameter point with this behavior and a value of a_μ in the allowed 2σ range was also defined and discussed in ref. [22].

Interplay of contributions to $a_{\mu e\gamma}$. For this case, the relevant flavor-violating amplitude is

$$a_{\mu e\gamma R} \approx -g_1 g_2 \frac{m_\mu^2}{48\pi^2 M_W \cos\beta} \frac{1}{M_1} N_{11}^* N_{13}^* \sum_m K_{m4}^* K_{m5} x_{1m} F_2^N(x_{1m}), \tag{4.26}$$

where sizable contributions come only from the slepton mass eigenstates containing mainly $\tilde{\mu}_R$ and \tilde{e}_R , which we label as $\tilde{\ell}_a$ and $\tilde{\ell}_b$, respectively. The mixing of the two states is given

²We use $N_{11} N_{13} \approx \frac{M_Z \sin\theta_W \sin\beta}{\mu}$, which is a good approximation if eq. (4.23) holds and in addition $|\mu| \gg M_Z$ and $\tan\beta \gtrsim 30$ [28].

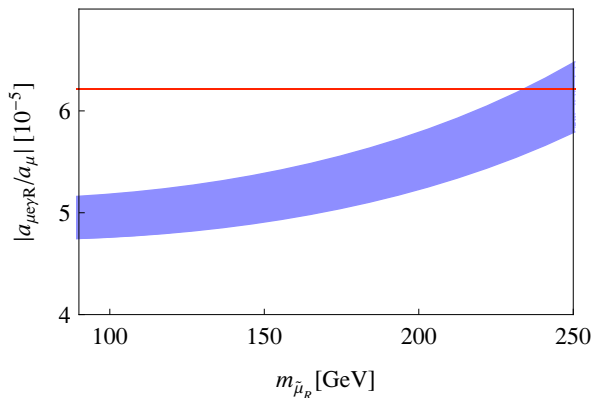


Figure 12. Correlation for the case of $\tilde{\mu}_R$ dominance. The band shows the ratio $|a_{\mu e \gamma R}/a_\mu|$ as a function of $m_{\tilde{\mu}_R}$, for a random variation of μ in the range $[-550, -650]$ GeV and M_2 in the range $[100, 900]$ GeV. The rest of the parameters are as in column IV of table 1. The approximation eq. (4.28) is represented by the horizontal line.

by $|K_{a5}K_{a4}| \approx |m_{\tilde{R}_{12}}^2 / (m_{\tilde{\ell}_a}^2 - m_{\tilde{\ell}_b}^2)|$ and $K_{b5}K_{b4} \approx -K_{a5}K_{a4}$ for real parameters. Using the same approximation for $N_{11}N_{13}$ as before, we find

$$|a_{\mu e \gamma R}| \approx g_1^2 \frac{m_\mu^2 \tan \beta}{48\pi^2 M_1 |\mu|} \left| m_{\tilde{R}_{12}}^2 \frac{x_{1a} F_2^N(x_{1a}) - x_{1b} F_2^N(x_{1b})}{m_{\tilde{\ell}_a}^2 - m_{\tilde{\ell}_b}^2} \right|. \quad (4.27)$$

Taking into account eq. (4.24), $|a_{\mu e \gamma R}/a_\mu|$ becomes

$$\left| \frac{a_{\mu e \gamma R}}{a_\mu} \right| \approx \left| \frac{m_{\tilde{R}_{12}}^2}{m_{\tilde{\ell}_a}^2 - m_{\tilde{\ell}_b}^2} \left(1 - \frac{x_{1b} F_2^N(x_{1b})}{x_{1a} F_2^N(x_{1a})} \right) \right| \sim \frac{|m_{\tilde{R}_{12}}^2|}{m_{\tilde{\ell}_b}^2}. \quad (4.28)$$

In figure 12 we show the numerical results for $|a_{\mu e \gamma R}/a_\mu|$ as a blue band, taking into account the chargino contribution as well. The parameters are set to the values of table 1, column IV; in particular, we varied μ in the range $[-550, -650]$ GeV and M_2 in the range $[100, 900]$ GeV. For $\mu < -650$ GeV, a_μ leaves the allowed 3σ region for the considered mass spectrum. Note that as long as the left-handed slepton masses are kept above 2 TeV, there is no change of the behavior presented for this scenario. The horizontal line in figure 12 represents the approximation of eq. (4.28). The width of the band in the figure and its limited variation with $m_{\tilde{\mu}_R}$ allow us to conclude that the case of neutralino- $\tilde{\mu}_R$ domination features a strong correlation between a_μ and $\text{BR}(\mu \rightarrow e\gamma)$.

5 Discussion and main results

5.1 Correlation between a_μ and $\text{BR}(\mu \rightarrow e\gamma)$ for similar supersymmetric masses

Our study started with the following basic question: assuming supersymmetric parameters that reproduce the observed value of a_μ , can we predict the amplitude $a_{\mu e \gamma L}$ (or $a_{\mu e \gamma R}$)? Evidently this amplitude depends on the flavor-violating parameter $m_{L_{12}}^2$ (or $m_{R_{12}}^2$), so in

the best possible case it would be proportional to a_μ times the dimensionless ratio of the flavor-violating parameter and some other SUSY mass $m_{\tilde{p}}^2$. I.e. in the best possible case we could write

$$\left| \frac{a_{\mu e \gamma L}}{a_\mu} \right| \approx f \frac{m_{\tilde{L}_{12}}^2}{m_{\tilde{p}}^2} \quad (5.1)$$

with a constant f . We found several parameter regions in which such correlations hold for $a_{\mu e \gamma L}$ or $a_{\mu e \gamma R}$, but the proportionality constant f and the appropriate mass ratio are specific for each region.

In section 4.1 we found that for similar masses of the supersymmetric particles involved in a_μ and $a_{\mu e \gamma}$, we can indeed determine the order of magnitude of $a_{\mu e \gamma L}/a_\mu$, employing as mass ratio the commonly used quantity $(\delta_{12}^l)_{LL}$ defined in eq. (4.2). The correlation is rather weak, however, and we also found that significant cancellations among different diagrams contributing to both processes are typical.

Nevertheless, using the MEG limit on $\text{BR}(\mu \rightarrow e \gamma)$ [13] we can put bounds on the flavor-violating parameters under the assumptions that a_μ is explained by SUSY and all relevant SUSY masses are similar. In the left panel of figure 13 we plot bounds on $(\delta_{12}^l)_{LL}$ as a function of $\tan \beta$. The bounds are obtained from a random scan as follows. For each value of $\tan \beta$, the value of the generic parameter M is chosen such that a_μ agrees with its central experimental counterpart in eq. (2.1) when

$$\mu = M_1 = M_2 = m_{\tilde{L}_{11}} = m_{\tilde{L}_{22}} = m_{\tilde{R}_{11}} = m_{\tilde{R}_{22}} = M. \quad (5.2)$$

Afterwards, random SUSY mass spectra are generated by varying the seven mass parameters above within the interval $[0.7M, 1.3M]$, imposing the conditions that (a) the LSP is a neutralino and (b) a_μ falls into the 1σ region given in eq. (2.1). From the generated spectra we derive three regions and two corresponding bounds on $(\delta_{12}^l)_{LL}$. The top-most (red) region in the left panel of figure 13 is “totally excluded”, i.e. $(\delta_{12}^l)_{LL}$ is so large that the MEG limit is violated by all generated mass spectra. The lower-most (green) region is “totally allowed”, i.e. the MEG limit is never violated. In the yellow region in between some (but not all) spectra satisfy the MEG limit. Thus, the upper, weaker bound delimiting the red region is conservative and must be satisfied (under the above assumptions). The yellow region is allowed by the above assumptions, but with more information on the SUSY masses from either experiment or theoretical models, the bound on $(\delta_{12}^l)_{LL}$ might go down as low as the lower, stronger bound delimiting the green region.

In order to see how the size of the mass range affects the bounds, we also investigate the smaller interval $(1 \pm 0.03) \times M$. The result is a narrower band limited by the dashed boundaries in the plot, which are analogous to the thick blue lines.

In addition to what is shown in the plot, we calculated bounds from a restricted set of spectra, imposing $m_{\tilde{L}_{11}} = m_{\tilde{L}_{22}}$ and $m_{\tilde{R}_{11}} = m_{\tilde{R}_{22}}$. In comparison to the general case, the additional degeneracy conditions result in a slightly relaxed strong bound. One can understand this from the fact that the conditions restrict the spread of $\text{BR}(\mu \rightarrow e \gamma)$ for a fixed mass insertion. By the same token, the weak bound becomes tighter, albeit only by a tiny margin.

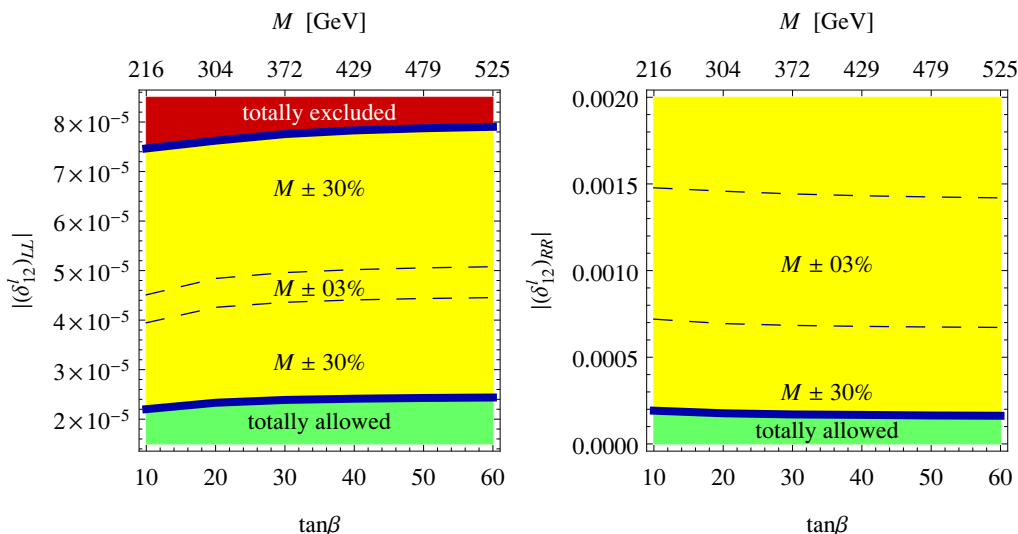


Figure 13. Strong and weak bounds on $(\delta^l_{12})_{LL}$ and $(\delta^l_{12})_{RR}$ for two different mass ranges: $(1 \pm 0.3)M$ and $(1 \pm 0.03)M$. See text for details.

In the right plot of figure 13, we consider flavor violation in the right-handed slepton sector. The weak bound on $(\delta^l_{12})_{RR}$ is not displayed. We omit it since the calculation is based on the approximation $\text{BR}(\mu \rightarrow e\gamma) \propto |(\delta^l_{12})_{RR}|^2$. Naively applying this relation would result in bounds of $\mathcal{O}(1)$. For so large values of $(\delta^l_{12})_{RR}$, the proportionality approximation is not valid. In any case, the weak bound is expected to lie far outside the plotted vertical range. For such a large mass insertion, it might not be $\text{BR}(\mu \rightarrow e\gamma)$ but the smallest slepton mass eigenvalue that determines the limit on $(\delta^l_{12})_{RR}$. For $|(\delta^l_{12})_{RR}| \ll 1$, one can always find a set of mass parameters within $[0.7M, 1.3M]$ such that different contributions to $\mu \rightarrow e\gamma$ cancel [29, 30], resulting in a decay rate below the MEG limit. The 3% range, however, is too narrow for a sufficient cancellation. This leads to the upper dashed curve, which depicts the weak bound for this small mass range.

After considering the case of similar superparticle masses, we turned to the next step, asking under which conditions a strong correlation arises. The answer is that there should be just one kind of diagram (where only one kind of supersymmetric particle mediates the contribution to both processes) and so we explored cases where either charginos or neutralinos could dominate.

5.2 Specific results for the case of chargino dominance

At the end of section 4.2 we have made a comparison between the accuracy of the correlations in cases where the charginos dominate both a_μ and $a_{\mu e\gamma}$ and the general correlation in the case of section 4.1. We have also pointed out for which cases the correlations become particularly useful. In summary, depending on the hierarchy of the sneutrino and chargino masses, the different approximations given in table 2 predict the ratio of the lighter chargino contributions to $a_{\mu e\gamma L}$ and a_μ , i.e. the ratio $a_{\mu e\gamma}^{\tilde{\chi}_k^\pm} / a_\mu^{\tilde{\chi}_k^\pm}$, within a factor 1.5, except for case IV. In cases I (for $M_2 \gtrsim 1 \text{ TeV}$), II, III, V, VI, and IX, these approxi-

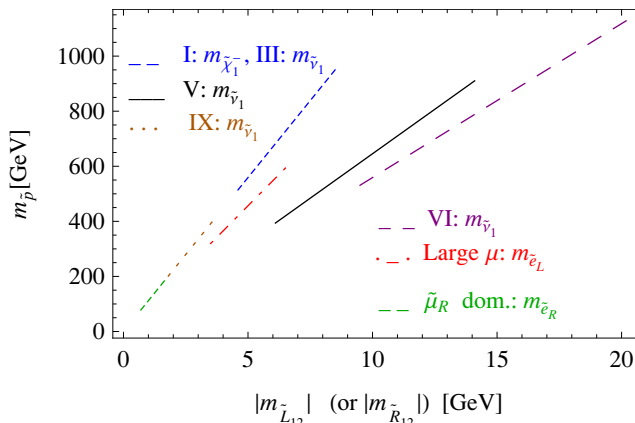


Figure 14. Lower bounds on the masses of the supersymmetric particles that drive the ratio $a_{\mu e\gamma L}/a_\mu$ as a function of the off-diagonal mass $m_{\tilde{L}_{12}}$ or $m_{\tilde{R}_{12}}$ for $\tan\beta = 50$. Cases I, III, V, VI and IX refer to the cases of chargino dominance, section 4.2, for which $m_{\tilde{L}_{12}}$ is relevant. For the case of large μ (where the neutralino contribution dominates), section 4.3, $m_{\tilde{L}_{12}}$ sets the bound for $m_{\tilde{e}_L}$ while $m_{\tilde{R}_{12}}$ sets the bound for $m_{\tilde{e}_R}$. The case of $\tilde{\mu}_R$ dominance, section 4.4, is only sensitive to $m_{\tilde{R}_{12}}$.

mations can even be used as a reliable substitute for the full value of $a_{\mu e\gamma L}/a_\mu$ stemming from all contributions.

Again, we can in turn use the obtained correlations to set bounds on the relevant parameter combinations appearing in $a_{\mu e\gamma L}/a_\mu$. In order to highlight the structure of the bounds and the differences in the different parameter regions we do not carry out scans in parameter space but we use the experimental information on a_μ from eq. (2.1) and require $\text{BR}(\mu \rightarrow e\gamma)$ to satisfy the bound (2.3). Then we obtain

$$\left| \frac{a_{\mu e\gamma L}}{a_\mu} \right| < 8 \times 10^{-5} \left| \frac{287 \times 10^{-11}}{a_\mu} \right|, \tag{5.3}$$

where we have omitted $|a_{\mu e\gamma R}|^2$ in the expression for $\text{BR}(\mu \rightarrow e\gamma)$ since it is subdominant. In all cases of table 2 in which the left-hand side can be approximated reliably as a simple mass ratio this bound translates into a lower bound on the corresponding mass $m_{\tilde{p}}$ of the supersymmetric particle driving the correlation between a_μ and $\text{BR}(\mu \rightarrow e\gamma)$; for example, for case I this is $m_{\tilde{\chi}_1^\pm}$. The bounds are functions of the flavor-violating parameter $m_{\tilde{L}_{12}}$. The results are shown in figure 14, where we have plotted only those cases of table 2 for which a reliable bound can be extracted. For each case we have restricted $m_{\tilde{p}}$ to the range where the approximation for $a_{\mu e\gamma L}/a_\mu$ is valid within a factor 1.5 and where a_μ can be made to lie in the favored 2σ region by choosing the superparticle masses appropriately. We can see that these requirements restrict considerably the scale $m_{\tilde{p}}$. In the figure $\tan\beta$ is fixed to 50; lowering (increasing) it would allow to loosen the lower (upper) bounds on $m_{\tilde{p}}$. Note that among the cases mentioned here, we have left out case II because the useful approximation involves logarithms and so it is not possible to set a bound on the mass of an individual particle.

5.3 Specific results for cases with neutralino dominance

We identified two particular regions of parameter space, also represented by the benchmark points 3 and 4 of refs. [22, 23], where neutralino contributions dominate and a_μ and $a_{\mu e\gamma}$ are strongly correlated.

If μ is very large and the bino mass M_1 sufficiently small, the exchange of the lightest, bino-like neutralino can become the dominant contribution. Contrary to what happens in the case of chargino dominance, for the neutralino case the contributions from $a_{\mu e\gamma R}$ can be relevant, since the lightest neutralino for this case is bino-like (see figure 8). Hence both left- and right-handed slepton contributions to $a_{\mu e\gamma}$ and to a_μ become important.

For this case, we have found in section 4.3 that indeed a single diagram dominates and there is a strong correlation between a_μ and $\text{BR}(\mu \rightarrow e\gamma)$. Hence we analyzed separately the correlations when either left-handed or right-handed charged sleptons dominate a_μ (and thus also $a_{\mu e\gamma}$). The correlations lead to relations of the type

$$\left| \frac{a_{\mu e\gamma L}}{a_\mu} \right| \approx \frac{2}{3} \frac{|m_{\tilde{L}_{12}}^2|}{m_{\tilde{\ell}_a}^2}, \quad \left| \frac{a_{\mu e\gamma R}}{a_\mu} \right| \approx \frac{2}{3} \frac{|m_{\tilde{R}_{12}}^2|}{m_{\tilde{\ell}_a}^2},$$

where $\tilde{\ell}_a \approx \tilde{e}_L$ and $\tilde{\ell}_a \approx \tilde{e}_R$, respectively. In this sense, just as in the case of chargino dominance, we can obtain reliable lower bounds on the mass of the supersymmetric particle driving the correlation between a_μ and $\text{BR}(\mu \rightarrow e\gamma)$. We plot the results in figure 14, where we can also compare to the bounds in the case of the chargino dominance.

Another case of neutralino dominance for which we have found a strong correlation is the case analyzed in section 4.4, where a_μ is dominated by diagrams involving the right-handed smuon and the lightest neutralino. The conditions for this dominance are that (a) left-handed slepton masses be much more bigger than $|\mu|$ and (b) $M_1, m_{\tilde{\mu}_R}, m_{\tilde{e}_R} < M_2$. We find that

$$\left| \frac{a_{\mu e\gamma R}}{a_\mu} \right| \sim \frac{|m_{\tilde{R}_{12}}^2|}{m_{\tilde{\ell}_a}^2},$$

where now obviously $\tilde{\ell}_a \approx \tilde{e}_R$. The lower bound on the mass of $\tilde{\ell}_a$, as a function of $|m_{\tilde{R}_{12}}^2|$, is also visualized in figure 14.

5.4 Comparison of different scenarios

Figure 15 summarizes the correlations found in the three most important cases. The plot displays three “islands”: (a) the similar supersymmetric masses case, section 4.1, (b) the case of large μ , and (c) $\tilde{\mu}_R$ dominance, for $\tan\beta = 50$ and $(\delta_{12}^l)_{LL} = (\delta_{12}^l)_{RR} = 2 \times 10^{-5}$. The mass ranges are as follows: for scenario (a) all the seven mass parameters vary between 300 GeV and 600 GeV. For case (b), M_1 varies as in (a), while the slepton masses vary between 450 GeV and 900 GeV, and $\mu = M_2$ are fixed at 4 TeV. Finally, for scenario (c) we have chosen $M_1 \in [100, 150]$ GeV, $M_2 \in [500, 2000]$ GeV, $-\mu \in [300, 600]$ GeV, $m_{\tilde{e}_R} \in [100, 200]$ GeV and $m_{\tilde{e}_L} = 3$ TeV. The figure confirms the existence of correlations, and it allows to easily look up the expected results for each parameter region. In detail, let us explain why we observe a slightly larger variation of $\text{BR}(\mu \rightarrow e\gamma)$ for fixed a_μ than

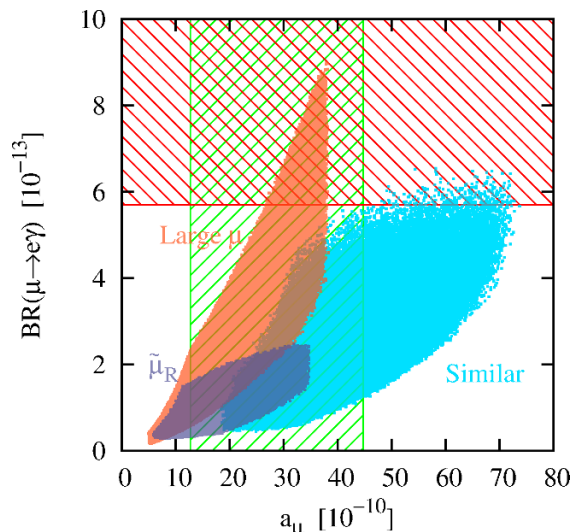


Figure 15. Comparison of the large μ and the $\tilde{\mu}_R$ dominance scenarios with the case of similar supersymmetric masses. See text for details.

found earlier, for example in figure 10. Earlier we fixed the very parameter ratio driving the correlation between a_μ and $\text{BR}(\mu \rightarrow e\gamma)$, for example $m_{L12}^2/m_{\tilde{\ell}_a}^2$. In figure 15 we fixed $(\delta_{12}^l)_{LL} \approx m_{L12}^2/m_{\tilde{\ell}_a}^2 \times m_{\tilde{e}_L}/m_{\tilde{\mu}_L}$, i.e. the decisive parameter multiplied by a factor varying between 0.5 and 2 if we vary the slepton masses between 450 GeV and 900 GeV. This illustrates a certain limitation of the correlations: even if we consider just a single diagram, varying all SUSY masses by a factor of 2 can still change the branching ratio by an order of magnitude, unless we fix the “correct” flavor-violating parameter, which varies from diagram to diagram.

Finally, let us compare our results to previous studies in the literature where stronger correlations were found. In particular, figure 6 of [3] shows a narrower band than the one for the case of similar supersymmetric masses plotted in our figure 15. To clarify, in the left panel of figure 16 we reproduce our results for the similar masses scenario together with the results of figure 6 of [3] using the same constraints as there, except A_U , which we set to zero, and $(\delta_{12}^l)_{LL}$, which we set to 2×10^{-5} . Specifically, in [3] the additional constraints with respect to ours are $M_2 \approx 2M_1$ and $m_{\tilde{L}_{11}} = m_{\tilde{L}_{22}} = m_{\tilde{R}_{11}} = m_{\tilde{R}_{22}}$. The resulting band is the black (darkest) one in our figure 16. Indeed it agrees with the corresponding one in ref. [3]. Relaxing the constraint on the gaugino masses produces a wider, dark blue (dark grey) band, and relaxing the constraints on the slepton masses produces the light blue (light grey) band. This shows that the correlation found in [3] is stronger than the one we find (for our similar supersymmetric mass scenario) because of the constraints on the slepton and gaugino masses.

Furthermore, the right panel of figure 16 displays an anatomy of the decorrelation effect arising from the variation of each parameter. First, we pick up a representative point, marked by the black dot, out of the black band in the left panel. Then, we vary each of the dimensionful parameters shown in the plot by a factor of 10 around the dot, for instance, $240 \text{ GeV} \leq \mu \leq 2400 \text{ GeV}$. The range of $\tan\beta$ is from 10 to 70. One might

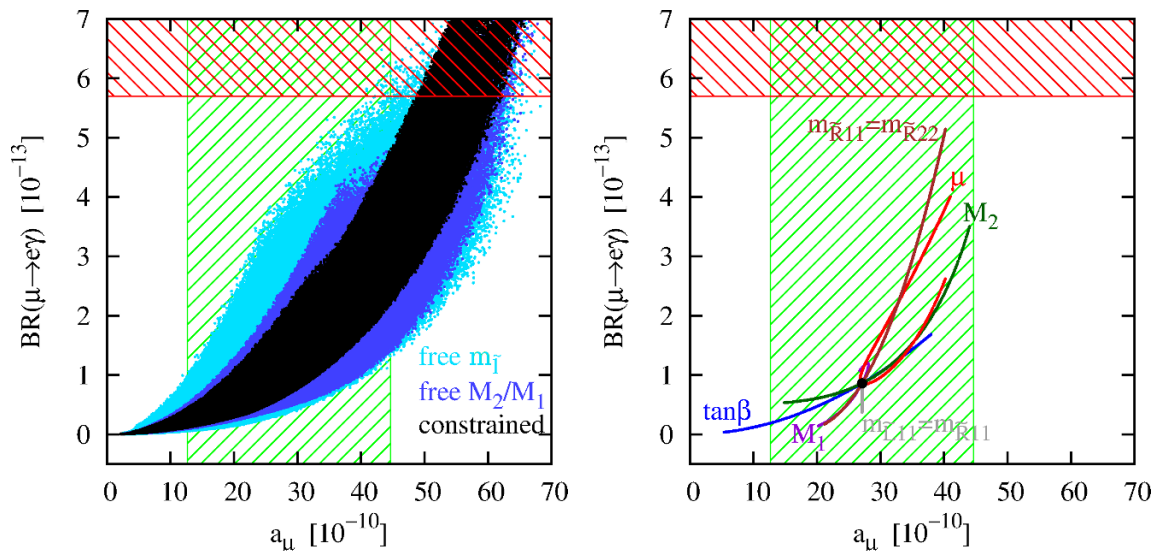


Figure 16. Left: comparison of the results found in [3] to our similar supersymmetric mass scenario. The parameter ranges are $300 \text{ GeV} \leq m_{\tilde{L}_{11}}, m_{\tilde{L}_{22}}, m_{\tilde{R}_{11}}, m_{\tilde{R}_{22}} \leq 600 \text{ GeV}$, $100 \text{ GeV} \leq M_1 \leq 500 \text{ GeV}$, $200 \text{ GeV} \leq M_2 \leq 1000 \text{ GeV}$, $500 \text{ GeV} \leq \mu \leq 1000 \text{ GeV}$, $10 \leq \tan\beta \leq 50$. The black band obeys the constraints $M_2 = 2M_1$, $m_{\tilde{L}_{11}} = m_{\tilde{L}_{22}} = m_{\tilde{R}_{11}} = m_{\tilde{R}_{22}}$. In the dark blue (dark grey) region, M_1 and M_2 are independent of each other. In the light blue (light grey) region, the four $m_{\tilde{L}_{ii}/\tilde{R}_{ii}}$ are independent of one another. Right: drift of a point due to the change of each variable, around the black dot with $\tan\beta = 50$, $M_1 = 300 \text{ GeV}$, $M_2 = 600 \text{ GeV}$, $\mu = 750 \text{ GeV}$, $m_{\tilde{L}_{11}} = m_{\tilde{L}_{22}} = m_{\tilde{R}_{11}} = m_{\tilde{R}_{22}} = 380 \text{ GeV}$.

regard the $\tan\beta$ curve as depicting the principal correlation that guides the black band, as both a_μ and $a_{\mu e\gamma L}$ are approximately proportional to $\tan\beta$. The other curves are then deviations from this principal correlation. Among them, the $m_{\tilde{L}_{11}} = m_{\tilde{R}_{11}}$ line should be the easiest to understand: it shows simply that a_μ remains fixed while $BR(\mu \rightarrow e\gamma)$ decreases as the selectron masses increase. One can notice in the left panel that relaxing the equality of the four diagonal slepton masses causes a greater spread than unfixing the gaugino mass ratio. In the right plot, the slepton mass splits are further divided into two classes: the intergeneration split and the left-right split. Comparing the $m_{\tilde{L}_{11}} = m_{\tilde{R}_{11}}$ and the $m_{\tilde{R}_{11}} = m_{\tilde{R}_{22}}$ curves, one finds that the left-right split causes a larger deviation from the principal correlation.

In conclusion, the essential goal of the present work was to characterize the sources of the possible correlation between a_μ and $BR(\mu \rightarrow e\gamma)$. We discerned that in the case of similar SUSY masses entering both observables cancellations are typical and hence the correlation is rather weak; we also identified some cases where the correlation is strong. In these cases we derived bounds on the flavor-violating parameters under various assumptions (figure 13) and conversely bounds on the masses of supersymmetric particles, as a function of only one flavor-violating parameter (figure 14). The ultimate application of this kind of analyses would be attained if $BR(\mu \rightarrow e\gamma)$ could eventually be measured, because that would give definite indications for the required values of all relevant mass parameters. Finally, figure 15 and figure 16 can be regarded as a summary, and as an update and

generalization of ref. [3]. The looser the assumptions in particular on slepton masses, the weaker the correlations, but there are interesting further parameter space islands with strong mass hierarchies, where correlations exist.

Acknowledgments

This work was supported by the German Research Foundation (DFG) via the Junior Research Group “SUSY Phenomenology” and an SFB Fellowship for L. Velasco-Sevilla within the Collaborative Research Center 676 “Particles, Strings and the Early Universe”. J.P. acknowledges support from the MEC and FEDER (EC) Grants FPA2011–23596 and the Generalitat Valenciana under grant PROMETEOII/2013/017. We thank Zackaria Chacko for discussions.

Open Access. This article is distributed under the terms of the Creative Commons Attribution License ([CC-BY 4.0](https://creativecommons.org/licenses/by/4.0/)), which permits any use, distribution and reproduction in any medium, provided the original author(s) and source are credited.

References

- [1] M. Graesser and S.D. Thomas, *Supersymmetric relations among electromagnetic dipole operators*, *Phys. Rev. D* **65** (2002) 075012 [[hep-ph/0104254](#)] [[INSPIRE](#)].
- [2] Z. Chacko and G.D. Kribs, *Constraints on lepton flavor violation in the MSSM from the muon anomalous magnetic moment measurement*, *Phys. Rev. D* **64** (2001) 075015 [[hep-ph/0104317](#)] [[INSPIRE](#)].
- [3] G. Isidori, F. Mescia, P. Paradisi and D. Temes, *Flavour physics at large $\tan\beta$ with a binolike lightest supersymmetric particle*, *Phys. Rev. D* **75** (2007) 115019 [[hep-ph/0703035](#)] [[INSPIRE](#)].
- [4] MUON G-2 collaboration, G.W. Bennett et al., *Final Report of the Muon E821 Anomalous Magnetic Moment Measurement at BNL*, *Phys. Rev. D* **73** (2006) 072003 [[hep-ex/0602035](#)] [[INSPIRE](#)].
- [5] M. Davier, A. Hoecker, B. Malaescu and Z. Zhang, *Reevaluation of the Hadronic Contributions to the Muon $g - 2$ and to $\alpha(M_Z^2)$* , *Eur. Phys. J. C* **71** (2011) 1515 [*Erratum ibid.* **C 72** (2012) 1874] [[arXiv:1010.4180](#)] [[INSPIRE](#)].
- [6] T. Aoyama, M. Hayakawa, T. Kinoshita and M. Nio, *Complete Tenth-Order QED Contribution to the Muon $g - 2$* , *Phys. Rev. Lett.* **109** (2012) 111808 [[arXiv:1205.5370](#)] [[INSPIRE](#)].
- [7] C. Gnendiger, D. Stöckinger and H. Stöckinger-Kim, *The electroweak contributions to $(g - 2)_\mu$ after the Higgs boson mass measurement*, *Phys. Rev. D* **88** (2013) 053005 [[arXiv:1306.5546](#)] [[INSPIRE](#)].
- [8] K. Hagiwara, R. Liao, A.D. Martin, D. Nomura and T. Teubner, *$(g - 2)_\mu$ and $\alpha(M_Z^2)$ re-evaluated using new precise data*, *J. Phys. G* **38** (2011) 085003 [[arXiv:1105.3149](#)] [[INSPIRE](#)].
- [9] M. Benayoun, P. David, L. DelBuono and F. Jegerlehner, *An Update of the HLS Estimate of the Muon $g-2$* , *Eur. Phys. J. C* **73** (2013) 2453 [[arXiv:1210.7184](#)] [[INSPIRE](#)].

- [10] NEW ($g - 2$) collaboration, R.M. Carey et al., *The New ($g - 2$) Experiment: A Proposal to Measure the Muon Anomalous Magnetic Moment to ± 0.14 ppm Precision*, FERMILAB-PROPOSAL-0989, FNAL (2009), <http://inspirehep.net/record/818866/files/fermilab-proposal-0989.PDF>.
- [11] B.L. Roberts, *Status of the Fermilab Muon ($g - 2$) Experiment*, *Chin. Phys. C* **34** (2010) 741 [[arXiv:1001.2898](#)] [[INSPIRE](#)].
- [12] J-PARC NEW G-2/EDM EXPERIMENT collaboration, H. Iinuma, *New approach to the muon $g-2$ and EDM experiment at J-PARC*, *J. Phys. Conf. Ser.* **295** (2011) 012032 [[INSPIRE](#)].
- [13] MEG collaboration, J. Adam et al., *New constraint on the existence of the $\mu^+ \rightarrow e^+ \gamma$ decay*, *Phys. Rev. Lett.* **110** (2013) 201801 [[arXiv:1303.0754](#)] [[INSPIRE](#)].
- [14] A.M. Baldini, F. Cei, C. Cerri, S. Dussoni, L. Galli et al., *MEG Upgrade Proposal*, [arXiv:1301.7225](#) [[INSPIRE](#)].
- [15] J. Hisano, T. Moroi, K. Tobe and M. Yamaguchi, *Lepton flavor violation via right-handed neutrino Yukawa couplings in supersymmetric standard model*, *Phys. Rev. D* **53** (1996) 2442 [[hep-ph/9510309](#)] [[INSPIRE](#)].
- [16] BAYESFITS GROUP collaboration, A. Fowlie, K. Kowalska, L. Roszkowski, E.M. Sessolo and Y.-L.S. Tsai, *Dark matter and collider signatures of the MSSM*, *Phys. Rev. D* **88** (2013) 055012 [[arXiv:1306.1567](#)] [[INSPIRE](#)].
- [17] M. Cahill-Rowley, J.L. Hewett, A. Ismail and T.G. Rizzo, *p MSSM Studies at the 7, 8 and 14 TeV LHC*, [arXiv:1307.8444](#) [[INSPIRE](#)].
- [18] S. Henrot-Versillé, R. Lafaye, T. Plehn, M. Rauch, D. Zerwas et al., *Constraining Supersymmetry using the relic density and the Higgs boson*, *Phys. Rev. D* **89** (2014) 055017 [[arXiv:1309.6958](#)] [[INSPIRE](#)].
- [19] L. Calibbi, J.M. Lindert, T. Ota and Y. Takahashi, *Cornering light Neutralino Dark Matter at the LHC*, *JHEP* **10** (2013) 132 [[arXiv:1307.4119](#)] [[INSPIRE](#)].
- [20] G. Bélanger, G. Drieu La Rochelle, B. Dumont, R.M. Godbole, S. Kraml et al., *LHC constraints on light neutralino dark matter in the MSSM*, *Phys. Lett. B* **726** (2013) 773 [[arXiv:1308.3735](#)] [[INSPIRE](#)].
- [21] M. Endo, K. Hamaguchi, S. Iwamoto and T. Yoshinaga, *Muon $g - 2$ vs LHC in Supersymmetric Models*, *JHEP* **01** (2014) 123 [[arXiv:1303.4256](#)] [[INSPIRE](#)].
- [22] H.G. Fargnoli, C. Gnendiger, S. Paßehr, D. Stöckinger and H. Stöckinger-Kim, *Non-decoupling two-loop corrections to $(g - 2)_\mu$ from fermion/sfermion loops in the MSSM*, *Phys. Lett. B* **726** (2013) 717 [[arXiv:1309.0980](#)] [[INSPIRE](#)].
- [23] H. Fargnoli, C. Gnendiger, S. Paßehr, D. Stöckinger and H. Stöckinger-Kim, *Two-loop corrections to the muon magnetic moment from fermion/sfermion loops in the MSSM: detailed results*, *JHEP* **02** (2014) 070 [[arXiv:1311.1775](#)] [[INSPIRE](#)].
- [24] T. Moroi, *The Muon anomalous magnetic dipole moment in the minimal supersymmetric standard model*, *Phys. Rev. D* **53** (1996) 6565 [Erratum *ibid.* **D 56** (1997) 4424] [[hep-ph/9512396](#)] [[INSPIRE](#)].
- [25] D. Stöckinger, *The Muon Magnetic Moment and Supersymmetry*, *J. Phys. G* **34** (2007) R45 [[hep-ph/0609168](#)] [[INSPIRE](#)].

- [26] M. Endo, K. Hamaguchi, T. Kitahara and T. Yoshinaga, *Probing Bino contribution to muon $g - 2$* , *JHEP* **11** (2013) 013 [[arXiv:1309.3065](#)] [[INSPIRE](#)].
- [27] P. Grothaus, M. Lindner and Y. Takanishi, *Naturalness of Neutralino Dark Matter*, *JHEP* **07** (2013) 094 [[arXiv:1207.4434](#)] [[INSPIRE](#)].
- [28] J.F. Gunion and H.E. Haber, *Two-body Decays of Neutralinos and Charginos*, *Phys. Rev. D* **37** (1988) 2515 [[INSPIRE](#)].
- [29] I. Masina and C.A. Savoy, *Sleptonarium: Constraints on the CP and flavor pattern of scalar lepton masses*, *Nucl. Phys. B* **661** (2003) 365 [[hep-ph/0211283](#)] [[INSPIRE](#)].
- [30] P. Paradisi, *Constraints on SUSY lepton flavor violation by rare processes*, *JHEP* **10** (2005) 006 [[hep-ph/0505046](#)] [[INSPIRE](#)].